Accepted Manuscript

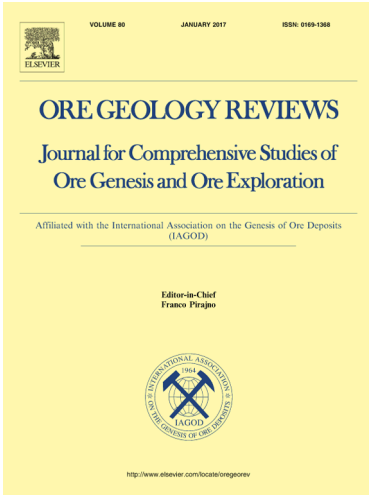

The Berezovsk Giant Intrusion-Related Gold Quartz deposit, Urals, Russia: Evidence for Multiple Magmatic and Metamorphic Fluid Reservoirs

Olga V. Vikent'eva, Nikolay S. Bortnikov, Ilya V. Vikentyev, Elena O. Groznova, Natalya G. Lyubimtseva, Valeriy V. Murzin

PII: S0169-1368(17)30529-2
DOI: http://dx.doi.org/10.1016/j.oregeorev.2017.08.018
Reference: OREGEO 2315

To appear in: *Ore Geology Reviews*

Received Date: 5 July 2017
Revised Date: 6 August 2017
Accepted Date: 10 August 2017

Please cite this article as: O.V. Vikent'eva, N.S. Bortnikov, I.V. Vikentyev, E.O. Groznova, N.G. Lyubimtseva, V.V. Murzin, The Berezovsk Giant Intrusion-Related Gold Quartz deposit, Urals, Russia: Evidence for Multiple Magmatic and Metamorphic Fluid Reservoirs, *Ore Geology Reviews* (2017), doi: http://dx.doi.org/10.1016/j.oregeorev.2017.08.018

The Berezovsk Giant Intrusion-Related Gold Quartz deposit, Urals, Russia: Evidence for Multiple Magmatic and Metamorphic Fluid Reservoirs

Olga V. Vikent'eva[a*], Nikolay S. Bortnikov[a], Ilya V. Vikentyev[a], Elena O. Groznova[a,b], Natalya G. Lyubimtseva[a], Valeriy V. Murzin[c]

[a]Institute of Geology of Ore Deposits, Petrography, Mineralogy and Geochemistry, Russian Academy of Sciences (IGEM RAS), 35 Staromonetny per., Moscow, 119017 Russia

[b]Institute of Experimental Mineralogy (IEM RAS) 4 Academica Osypyana ul., Chernogolovka, Moscow region, 142432 Russia

[c]Zavaritsky Institute of Geology and Geochemistry (IGG UB RAS), Russian Academy of Sciences, 15 Academica Vonsovskogo ul., Ekaterinburg, 620016 Russia

Dedicated to the memory of Prof. V.N. Sazonov, a great Russian scientist in the field of gold-bearing altered rocks of the Urals.

ABSTRACT

The Berezovsk gold deposit in the Middle Urals has been mined for 270 years. Its endowment (past production and gold reserves) is estimated to be 450 t of gold. The deposit is located in the greenschist metamorphosed Silurian volcanogenic-sedimentary rocks intruded by granitoid dykes to the north-east of Late Carboniferous Shartash granite massif. Mineralisation is represented by sulphide-quartz veins in the granitoid dykes ("ladder" veins) and in the host rocks ("krassyk" veins) formed in the following four stages: ankerite-quartz, quartz-pyrite, gold-polymetallic and carbonate. Ore veins are accompanied by halos of gumbeite (quartz + orthoclase + carbonate), beresite (quartz + sericite + ankerite + pyrite) and listvenite (quartz + Fe-Mg carbonate + fuchsite +pyrite). The veins mainly consist of quartz with sulphide minerals (commonly 3-5 vol. %). About 180 minerals have been identified in ores, but the most abundant minerals are quartz, calcite, ankerite, pyrite, galena, tennantite, chalcopyrite, aikinite, native gold, and sphalerite. Native gold was deposited during quartz-pyrite (Au I) and gold-polymetallic (Au II) stages. Fineness of gold ranges from 863 to 984 and from 723 to 848 for Au I and Au II, respectively. The mineral and metal zoning was identified relative to the roof of the Shartash granite massif. The fluid inclusion study revealed that the gold mineralisation at the Berezovsk deposit was formed at 300 to 230°C and 0.3 to 2.3

kbar (mostly 0.5 to 1.2 kbar), from a H_2O-CO_2-NaCl fluid with salinity of 7.3 to 18.2 wt % NaCl equiv. The fluid was separated into H_2O-CO_2-NaCl and CO_2-rich fluids due to temperature and/or pressure drop at the deposition site. Calculated $\delta^{18}O$ and δD values are 5.2 to 8.1‰ and –39 to –63‰, respectively, for the fluid in equilibrium with alteration assemblages. The average $\delta^{13}C$ value for the fluid equilibrated with carbonates from the inner zones of metasomatic halos is –5.3‰. The calculated $\delta^{18}O$ and $\delta^{13}C$ values are 3.0 to 9.6‰ and –3 to –9‰, respectively, for ore-forming fluids. The $\delta^{34}S$ values are 1.4 to 12.9‰ and –1.6 to 11.7‰ for the fluid in equilibrium with early and late sulphides, respectively. In addition to the isotopic data, the geological, mineralogical and fluid inclusion data confirmed the predominant contribution of the magmatic fluid to formation of the Berezovsk hydrothermal system. The light C, O, and S isotope enrichment of the fluid was mainly caused by fluid phase separation. Fluids generated by decarbonation and dehydration reactions due to the contact metamorphism of the host rocks during the Shartash massif emplacement were responsible for additional ^{34}S input. The ore-forming fluid was enriched in the light ^{16}O isotope on the deposit flanks indicating the mixing with heated meteoric water.

1 INTRODUCTION

The giant Berezovsk (also sometimes spelled as Berezovskoe) gold deposit (57°51'N-60°44'E) is located near the town of Berezovsk, 12 km east of Ekaterinburg (Fig. 1). The Berezovsk deposit was discovered in 1745. This initiated the beginning of the gold mining industry in Russia. It is a large gold deposit and it has been a major gold producer in Russia for more than two centuries, until the end of the 1950s. Historical production of gold (combined placer and bed rock metal) is estimated at 400 t. Numerous auriferous veins of the deposit have been completely worked out to the depth 100-250 m from surface. Significant reserves have been identified by the shafts between the 520-m and 750-m-levels. A peak of annual gold production, namely 2.6 t, was reached in 1937. Between 1970 and 1990 annual production was up to 2 t. The remaining probable and proved gold reserves of the deposit (approved in 2014) were 60.3 t and 30.2 t, respectively (Khramov, 2014). According to deep structural drilling data, the economically important ores occur to a depth of 1-1.2 km in the centre and on the northern flank of the deposit.

The Berezovsk granitoid dyke-hosted gold-quartz vein deposit was considered as a typical representative of the mesothermal vein gold-quartz deposits, spatially and genetically related to granitoid magmatism (Petrovskaya, 1972; Borodaevskaya,

Rozhkov, 1974; Boyle, 1979; Sazonov et al., 2001). During the last decades, such deposits were reclassified as intrusion-related gold deposits (e.g., Sillitoe and Thompson, 1998; Lang et al., 2000; Hart, 2005), and Berezovsk deposit was included into this deposit style. Some researchers (Goldfarb et al., 2005; Herrington et al., 2005) classified the Berezovsk deposit as orogenic according to the recent geodynamic reconstruction as well as location of gold-bearing veins both inside granitoid dykes and metamorphic host rocks of greenschist facies. At first, fluid sources were different for these two deposit styles; igneous source predominated for intrusion-related gold deposits, but metamorphic source was more probable for orogenic gold deposits. In recent years, multiple fluid source was recognised for both of these deposit styles (Tomkins, 2013; Goldfarb and Groves, 2015; Goryachev and Pirajno, 2016). Several sources of the hydrothermal fluid, including magmatic (e.g., Burrows et al., 1986; Hedenquist and Lowenstern, 1994), metamorphic-derived (e.g., Kerrich and Fyfe, 1981; Wilkinson, 1990; Phillips and Powell, 2010; Yardley and Cleverley, 2013; Goldfarb and Groves, 2015), and deeply circulating heated meteoric (e.g., Knopf, 1929; Nesbitt et al., 1986; Shelton et al., 1988) water were discussed for gold deposits.

The origin of ore-forming fluid is most debatable for the Berezovsk gold deposit (Bortnikov et al., 1997, 1998; Sazonov, 1999; Baksheev et al., 2001; Kryazhev et al., 2011). The fluid with dissolved components and metals derived directly from a magma source, as well as the fluid generation and mobilisation of its components by dehydration and decarbonation at contact–regional metamorphism have been proposed (Bortnikov et al., 1997, 1998).

The comprehensive geological, mineralogical, fluid inclusion and stable isotope study has been carried out to determine the composition of the fluid responsible for gold-quartz mineralisation at the Berezovsk deposit and possible sources of the mineralising fluid and solutes.

2 GEOLOGICAL SETTING

2.1 Regional geology

The Berezovsk deposit is located within the East Uralian zone to the east of the Tagil and Magnitogorsk zones (Ivanov et al., 1975; Sazonov et al., 2001; Brown et al., 2008) (Fig. 1). In the Middle Urals, the East Uralian zone is separated from the Tagil zone by the Serov-Mauk serpentinitic melange confined to the transpressional fault system (Puchkov, 1997; Ayarza et al., 2000; Brown et al., 2002). Both East Uralian and Tagil zones are parts of the Uralian orogenic belt, a Palaeozoic orogen between the

East European craton and the Altaid orogenic collage (Yakubchuk et al., 2002; Herrington et al., 2005; Puchkov, 2017; Yakubchuk, 2017). Its formation began from the collision of the Tagil intra-oceanic arc with the present eastern margin of the East European craton (e.g., Puchkov, 2017). The subsequent development of the orogen to the east of this arc involved the accretion of additional oceanic and microcontinental terranes. The southern part of the East Uralian zone mainly consists of greenschist to amphibolite-facies metapelites and is believed to represent the Precambrian continental crust (Puchkov, 1997, 2000) or Berezovsk microcontinent (Yazeva, Bochkarev, 1996), or part of the Kazakhstan plate (Brown et al., 2006).

Diachronous epicontinental volcanic arcs were probably formed at the active margin of the above mentioned continent during the Famennian to the Moscovian. Granite rocks formed medium-size batholiths, roughly circular or NS-elongated in shape (Bea et al., 1997, Fershtater, 2013). They were considered to be related to the two subduction zones (Bea et al., 1997; Brown et al., 2008, Fershtater et al., 2010). First, the subduction-related magmatism occurred between 370 Ma and 350 Ma in the eastern sector of the East Uralian zone. This phase of magmatism was interpreted (Bea et al., 2002) to have been related to the east-dipping subduction zone located to the east of the accreted Magnitogorsk arc producing the I-type granitoid batholiths. A second phase of subduction magmatism found in the western part of the East Uralian zone occurred from about 335 Ma to 315 Ma and was related to a subduction zone located to the east of the accreted Tagil arc. This zone dipped eastward underneath the older continental arc. I- and M-type granitoid batholiths were formed during this phase. Magmatic activity directly related to subduction was terminated before the Permian (Bea et al., 2002; Brown et al., 2006).

Most quartz-vein gold deposits in the Urals are spatially associated with Devonian and Carboniferous gabbro-tonalite-granodiorite-granite (GTGG) plutons which were formed in supra-subduction setting at the Andean-type continental margin (Koroteev et al., 1997; Sazonov et al., 2001; Fershtater, 2013). The Carboniferous Verkhiset and Shartash plutons consist of mildly peraluminous granitoids formed in relation to the subduction system, which was active in the Late Carboniferous. These granitoids with high SiO_2 and elevated Rb, Cs, Ba, Th and U contents were generated due to recycling of the older continental-arc rocks that were deeply buried during the collision. Such granitoids resulted from the crustal melting due to combination of radiogenic heating of an overthickened sialic crust, local underplating by mafic magmas, and local accumulation of heat and fluids related to the oblique crustal-scale strike-slip shearing

that finally assembled the Uralides (Bea et al., 2002). The Berezovsk gold deposit is associated with the Shartash granite pluton (Fig.1). This massif belongs to the Verkhiset magmatic area and is part of a chain of Carboniferous GTGG intrusives (Sazonov et al., 2001; Fershtater et al., 2010).

The gold mineralisation of the Berezovsk deposit is spatially related to the tonalitic Carboniferous granite and dykes of granite-porphyry injected into regionally metamorphosed greenschist rocks. The district consists of the rock complexes originated at different environments (Fig.1). Basalt and volcaniclastic sediments (Lower Silurian) and gabbro-ultramafic rocks (Early Silurian) are interpreted as relics of an early island arc complex. The significant part of the district consists of Carboniferous granodiorite, adamellite and granite believed to be emplaced at an active continental margin (Koroteev et al., 1997; Puchkov, 2017). This active continental margin regime evolved to continent/continent “hard” collision after the closure of Uralian palaeo-ocean during the Late Carboniferous to Early Permian times (Puchkov, 2000; Fershtater, 2013).

Two major regional fault systems were recognised in the area. The Murzinka S-N trending fault sited 15 km to the east from the Berezovsk deposit (see Fig. 1) is a steeply dipping shear zone up to 1.5 km in width. It subdivides the second-order fold- and block-structures. The Pyshma-Berezovsk fault zone restricts the deposit in the north. It extends from the west to the east and dips gently to the north at 30-45^{o}. The slab-like subvolcanic bodies of micro-gabbro as well as Pyshma gabbro-serpentinite massif are confined to this fault zone.

A regional scale metamorphism of country rocks is related to the collision events. Three types of metamorphic rocks were distinguished: (1) greenschist to epidote-amphibolite metamorphosed volcanic and volcanic-sedimentary rock; albite, chlorite, epidote, quartz, actinolite and sericite are dominant minerals in these rocks, with rare biotite, hematite and rutile; (2) apoharzburgitic serpentinite, with chrysotile and brucite as major constituents; (3) talc-carbonate rock in the serpentinite bodies; talc, chlorite and Fe-Mg-carbonate are dominant minerals (Sazonov et al., 2001).

2.2 Local Geology

The Berezovsk deposit is located within the area between Verkhiset granite batholith (Carboniferous, Bea et al., 2002) to the west and Precambrian (?) Murzinka granite-gneiss block to the east (Fig. 1). The deposit area consists of the Lower Silurian island-arc complex intruded by the Shartash granitoid pluton and granitoid porphyry

dykes (Sazonov et al., 1993, 2001). This complex consists of primitive high-Ti basalt lava, tuffite and siliceous metasediments with sub-concordant large lens-like massifs and small tectonic lenses of serpentinised harzburgite and gabbro. The stratified section is subdivided into three units: the lower (ore-bearing) unit (Lower Wenlock) consists mainly of interlaying basalt lava, tuff-breccia, tuffite and siliceous sediment; the middle unit is composed by basalt (Middle Wenlock), and the upper unit comprises terrigenious sedimentary rock (Upper Silurian). This volcanic-sedimentary sequence was metamorphosed to the greenshist facies and the rocks were transformed into epidote-actinolite-chlorite, chlorite-sericite-quartz, epidote-actinolite-sericite-quartz, epidote-chlorite-sericite and quartz-epidote-chlorite schists. Minor chert, phyllite and sandstone were also found. The thickness of this sequence exceeds 2 km.

The Shartash granite massif outcrops in the core of the Shartash brachianticline structure at the south-western flank of the ore field as a nearly isometric body of 6 x 8 km in size (Fig. 1) but it is part of the so-called Shartash batholith, 20 km in width. Host volcano-sedimentary and sedimentary sequences, dipping gently to the north and NE, constitute the limbs of the Shartash brachianticlinal structure (Fig. 2). These formations are crosscut by EW-trending thrusts and NS-trending strike-slip faults. Geophysical data (Bellavin et al., 1970) indicate that the hidden batholith has a cupola-like shape and relatively gentle north, north-east and east contacts; its roof occurs under the centre of the deposit at a depth of 2.5 to 3 km (Fig. 2). This multiple massif consists of three phases of biotitic granite-adamellite and minor granodiorite. Contents of Zr, Hf, Ba, Sr, and REE significantly increase from early to late granite phases. Granitoids of Shartash massif are very similar to the late tonalite-granodiorite and adamellite-granite series in the Verkhiset batholith, but are relatively enriched in lithophile (Li, Cs, Rb, Sr, Ba, Th, Zr, Hf) and chalcophile elements (Fershtater et al., 2010). The U-Pb (SHRIMP) dating of zircon from second phase of Shartash granite yielded a concordant age of 302±3 Ma (Pribavkin and Pushkarev, 2011).

The Shartash massif is accompanied by ~350 granitoid dykes represented by granodiorite-porphyry, granite-porphyry, quartz diorite, leucogranite, alaskite, aplite, granite-pegmatite and minor lamprophyre (kersantite and late minette). Granite-porphyry is predominant. The dykes are 3-10 km in length and ca. 10 m in thickness. Mostly NS-trending dykes reveal a vertical to steep dip and compose a fan-shaped dyke swarm relative to the roof of the Shartash massif (Fig. 2). The cross-cutting relations between the dykes of different composition suggest their intrusion during two episodes (Borodaevskii and Borodaevskaya, 1947; Sazonov et al., 2001). Eight zircon grains

from granite-porphyry dyke of the early episode, studied with SHRIMP-II, revealed a $^{206}Pb/^{238}U$ concordant age of 305±7 Ma (Pribavkin and Pushkarev, 2011). These data show similar crystallisation ages of granite and granite-porphyry dyke. Lamprophyre dyke with $^{40}Ar/^{39}Ar$ age for the phlogopite phenocrysts at 284.4±3.6 Ma age (Pribavkin et al., 2007) cross-cuts the sulphide-quartz veinlets.

2.3 Geology of veins

The Berezovsk deposit consists of early tungsten-bearing scheelite-quartz-tourmaline veins and late gold-bearing sulphide-quartz veins (Borodaevskii and Borodaevskaya, 1947). *Scheelite-quartz-tourmaline* veins occur in the granite of the Shartash massif and extend into volcanogenic-sedimentary rocks for up to 3 km from its contact. These nearly east-west to rare northwest-trending veins dip to the south or northeast (30-50°). The length along strike and the thickness range from 50 to 200 m and 0.1 to 2.5 m, respectively. Grey massive quartz is a dominant gangue mineral. Scheelite comprises bands along the vein selvages and pockets. These veins are crosscut by the auriferous veins.

Gold-sulphide-quartz veins are of the most economic importance. They can be subdivided into two types. The veins of the first type, named “ladder” or “lestnichnye” (term used by the Russian prospectors), occur within the granitoid dykes (Fig. 3, 4). This is a specific feature of the Berezovsk deposit. Several tens of thousands of such ladder veins, mainly oriented orthogonally to dyke contacts, were delineated. Their dominant strike is 90-110°, and they dip to the south (70-80°) or rarely steeply northward. There are several morphological types of ladder veins: (1) major WE-trending and steeply dipping veins, 20 to 35 m long filling the extensional fractures; (2) WE-trending, gently northward dipping veins, up to 50 m along shear fractures; (3-4) two systems of gently dipping oblique shear-related veins striking 135° SE and 45° NE; (5) relatively short veins occurring along dyke contacts were controlled by strike-sleep deformations (Sazonov, 1975). The length of veins is restricted to the thickness of dykes and varies from 2.2 to 8.7 m, their width is 3 to 12 m. The vein thickness ranges from 2 to 60 cm, rarely up to 100 cm. Each dyke commonly contains about 15 veins per 10 m of its length; sometimes the veins form stockwork in the dyke.

The second type of veins includes those located (Fig. 5) in volcanogenic and sedimentary rocks as well as in serpentinite transformed into talc-carbonate rock. These veins are locally named as “krassyk” veins because of the red colour (“krasnyi” in Russian) of the weathered enclosing rock. About 400 east-west-trending high-angle,

rarely low-angle south-dipping “krassyk” veins are located mainly in the north and east, as well as in the centre of the deposit. They form swarms of 4-10 veins, up to 40 m long. The total length of such en echelon clusters is usually of 200 to 300 m, rarely up to 1 km. Some of the “krassyk” veins are related to the ladder veins being their continuation. Two east-west-trending zones of the “krassyk” veins are recognised: (1) the northern 2-km wide zone occurring in serpentinite and gabbro includes main economically significant auriferous veins; (2) the southern 1-km wide zone is hosted by metabasalt.

2.4 Wall-rock alteration

Three hydrothermal alteration assemblages were recognised at the Berezovsk deposit: barren propylite, tungsten-bearing gumbeite and gold-bearing beresite-listvenite.

Propylite (actinolite, albite, chlorite, calcite, quartz and pyrite), formed before the dykes of granite-porphyry, has significant areal extent and associates with fault zones (Sazonov, 1975). The veins within the propylitic rock contain quartz, magnesite, talc, tourmaline and chrome-bearing muscovite.

Gumbeite (quartz, orthoclase, dolomite, phlogopite, pyrite, and scheelite) occurs around scheelite-bearing veins on the southern flank of the field near the Shartash massif (Shartash tungsten occurrence, Spiridonov et al., 1998).

Beresite-listvenite is the main type of alteration adjacent to auriferous veins of the Berezovsk deposit (Sazonov, 1975; Sazonov et al., 2001). It was first described at this deposit by Rose (1837) (Fig.7). This alteration is a result of acidic metasomatism (beresitisation) in ultrabasic rocks (listvenite) and granitoid rocks (beresite). Beresite named after the Berezovsk deposit altered the granite-porphyry. It consists of quartz, sericite, carbonate (typically ankerite) and pyrite. The alteration halo displays a zonal distribution of mineral assemblages relative to the vein: biotite-microcline-albite-quartz-calcite-magnetite (outer zone), microcline-albite-quartz-dolomite-muscovite-pyrite, albite-quartz-ankerite-muscovite-pyrite, quartz-ankerite-sericite-pyrite (inner zone).

Listvenite named after the Russian word “listva” (foliage) has green colour like foliage. It altered serpentinite, gabbro and basalt. A zoning of listvenite replaced gabbro is as follows: the outer zone consists of actinolite, epidote, chlorite, plagioclase, calcite; the intermediate one is composed of chlorite, albite, dolomite-ankerite and quartz; the second intermediate zone consists of dolomite-mesitite, quartz and muscovite; carbonate minerals (dolomite, mesitite, and ankerite), quartz, and mica (muscovite, paragonite, and fuchsite) form the inner zone. Altered basalt has the following

metasomatic zones: actinolite-epidote-chlorite-albite-calcite-(biotite) (outer zone), chlorite-albite-dolomite or ankerite-muscovite-quartz, albite-ankerite-muscovite-quartz, ankerite-sericite-quartz (inner zone). The outer zone of listvenite superimposed on serpentinite consists of talc, chlorite, breunnerite and chromite, while the zones near the veins consist of quartz-breunnerite or quartz-magnesite assemblages with fuchsite, chromite and pyrite.

The altered granite contains disseminated pyrite, forming crystals of cubic, pentagondodecahedral, and octahedral habits among the quartz-sericite-ankerite aggregate. These disseminated ores are of economic importance: gold grade is up to 5 g/t (average 1.3 g/t) and ores contain about 35% of total Au reserves.

3 MINERALOGY AND PARAGENESES OF VEINS

Quartz veins are a principal source of gold that contributed more than 65% of total gold production. The average gold grade is 18-20 g/t. Amount of sulphide minerals in the veins does not exceed 10 vol. % (commonly 3-5 vol. %). About 180 minerals have been found in the ores of the Berezovsk deposit (Table 1). The most abundant minerals of the veins are quartz, calcite, ankerite, pyrite, galena, tennantite, chalcopyrite, aikinite, native gold, and sphalerite. Other minerals are extremely rare.

3.1 Sequence of mineral formation.

Textural and structural relationships between mineral aggregates, crystal habits, grain size of minerals indicate that the minerals of the veins were crystallised during four stages: 1) early, ankerite-quartz; 2) pyrite-quartz; 3) gold-polymetallic; and 4) late, carbonate stage (Fig.8). In the text below, the roman numbers I, II, III correspond to the mineral generations.

Ankerite-quartz stage

Mineral aggregates of this stage fill the fractures both in the granitoid dykes and outside of these dykes. Quartz and ankerite are main minerals of the stage. Early ankerite was replaced by quartz. Semi-milky coarse-grained quartz with abundant drusy vugs fills tension cracks. Shears are filled with medium-grained quartz without druses. Pyrite I crystals, 1 to 10 mm (sometimes, up to 5 cm) in size, occur irregularly among the mineral aggregates of this stage.

Pyrite-quartz stage

Quartz and pyrite are dominant minerals deposited during this stage. Pyrite II occurs commonly as cubic crystals, rarely as pentagondodecahedron. The size of these crystals is less than those deposited during the first stage. Fine-grained quartz was formed probably as a result of re-crystallisation of early quartz. The quartz veinlets frequently cross the mineral aggregates of the early stage. Scheelite and native gold I are less common minerals in this stage. Scheelite occurs as aggregates of crystals or isolated grains within quartz. Small inclusions of native gold were recorded inside the pyrite crystals and in intergranular spaces within the pyrite-quartz aggregate. Chalcopyrite I, galena I and sphalerite I occur sporadically. Chalcopyrite I fills intergranular spaces and fractures in pyrite and quartz (Fig. 9). Sphalerite I crosses chalcopyrite I and forms inclusions in the centre of pyrite crystals. Galena I fills cracks and interstices in pyrite II. Curved crystals of galena I were found and galena injection into beresite was observed.

Gold-polymetallic stage

The main minerals deposited during this stage are pyrite, tennantite, chalcopyrite, sphalerite, galena, Bi sulphosalts (aikinite, matildite, bismuthinite, cosalite) and native gold (Fig. 10). Pyrite III forms cracked aggregate, rarely well-shaped crystals and contains isometric inclusions of tennantite and native gold II. Numerous cracks in pyrite are commonly filled with chalcopyrite II, tennantite, galena II and native gold II that indicate their later deposition. Isometric inclusions of chalcopyrite II were found in tennantite, sphalerite II and galena II. Chalcopyrite II overgrows and crosses tennantite. Galena II corrodes pyrite III. There is an evidence of mutual replacements between galena and tennantite. Matildite occurs as rims on chalcopyrite II in the galena veinlets. Sphalerite II contains stringers and blebs of chalcopyrite II. Aikinite is associated with matildite, galena II, gersdorffite and forms inclusions in chalcopyrite II and tennantite. Native gold II occurs as fine (1-11 μm) inclusions isometric as well as irregular shapes and stringers within pyrite and tennantite-tetrahedrite minerals. It commonly associates with xenomorphic and vein-like isolations of chalcopyrite II in tennantite. The principal minerals hosting the native gold inclusions are pyrite (46%) tennantite (39%), chalcopyrite (12%) and galena (2%). Three gold-bearing mineral assemblages of this stage are recognised: 1) pyrite III – native gold II; 2) tennantite – native gold II – galena – aikinite – matildite; 3) chalcopyrite II – sphalerite II – native gold II ± aikinite. A lot of large native gold crystals in quartz has been discovered at the northern flank of the Berezovsk deposit at the 520 m level. The largest of them has a weight of 600 g. The

large native gold has been found in the ladder quartz vein in its pinching out at the contact of Pervopavlovskaya plagiogranite-porphyry dyke with aposerpentinitic listvenites (Murzin et al., 1987). The mineral composition of the gold-polymetallic stage is not uniform. It becomes more complicated from the bottom to the top (levels from 462 to 169 m). At a depth of 462 to 314 m, the main minerals are pyrite and chalcopyrite; tennantite, galena and sphalerite are extremely rare. At a shallow depth (from 212 to 169 m), sulphosalts are found in addition to abundant pyrite, chalcopyrite and tennantite, although galena and sphalerite are rare.

Carbonate stage

Calcite is dominant and dolomite is rare for the stage. The calcite veins cross the earlier aggregates of sulphides and quartz. Druses of calcite grew on the earlier minerals. Free gold has not been found in the assemblages of this stage.

3.2 Mineral chemistry and zoning

The chemical composition of tennantite-tetrahedrite, native gold and sphalerite has been studied in details using electron probe microanalysis, taking in mind that the mineral solid solutions are sensitive indicators of deposition conditions and temporal and spatial evolution of fluids.

Native gold

Native gold in pyrite-quartz (Au I) and gold-polymetallic (Au II in intergrowths with pyrite and tennantite) assemblages of veins has been examined. Silver is a major admixed component in native gold. Another trace element in the most of gold grains is copper. The exception is Au II in pyrite, where the Cu content is below 0.02 wt. %. Fineness of Au I ranges from 863 to 984 (average 934), while fineness of Au II lies within 723 – 848 (the mean value for Au II included in pyrite is 797 and that found inside of tennantite is 851) suggesting that its fineness decreases from early to the late generation (Fig. 11). Inspection of samples collected from different levels of the deposit indicates that the native gold fineness increases to the east and to the south, especially for the late generation (Table 2). The fineness of early native gold decreases and of late native gold increases with the depth. Composition of coexisting minerals has been examined. The native gold fineness raises (and Ag content falls) and the Sb and Ag contents in coexisting tennantite minerals increase from the north to the south and with the depth. Mineral formation temperatures calculated on the basis of tennantite and

native gold (Au II) composition using the geothermometer by Sack (Sack and Brackebusch, 2004) are 174 to 208°C.

Tennantite-tetrahedrite minerals

The major elements in the tennantite-tetrahedrite minerals at the Berezovsk deposit are Cu, Fe, Zn, As, Sb and S, while Ag, Bi, and Hg are minor constituents. In general, arsenic is a dominant semi-metal in tennantite-tetrahedrite minerals (about 180 analyses). Thus, this mineral is identified as tennantite. Tetrahedrite was found only on the southern flank of the ore field (Chesnokov, 1973). The Sb/(Sb+As+Bi) ratio in these minerals varies from 0.02 to 0.5 and increases from the north to the south (Fig. 12). The (Fe/Fe+Zn) ratio in tennantite varies from 0.2 to 0.71 and increases towards the west and north. Tennantite of the Berezovsk deposit contains low concentration of silver that ranges from 0.05 to 0.9 wt. % and tends to increase toward the south. Significant positive correlation (r=0.8) between Ag and Sb content in tennantite was revealed. The mineral from southern flank of the deposit contains minor bismuth concentrations, ranging from 0.13 to 3.57 wt. % and increasing with depth, while Hg-bearing tennantite was found on the northern flank.

Sphalerite

Sphalerite contains minor concentrations of Fe, Cd and Cu. Low iron content (0.12-0.76 wt. %) is a characteristic feature of sphalerite at this deposit. The Cd content varies from 0.14 to 0.9 wt. %. Higher Cd content in sphalerite (up to 0.9 wt. %) has been found in the south and in the east. The Cd content increases with depth (from 0.1-0.5 to 0.6-0.7 wt. %). The Cu content ranges from 0.07 to 0.98 wt. % and decreases from the upper to deeper levels (from 0.56-0.98 to 0.07-0.17 wt. %).

Electron microprobe analyses show a direct relationship between iron content in coexisting sphalerite and tennantite-tetrahedrite minerals. Chemical composition of coexisting tennantite and sphalerite II was used to estimate the formation temperatures of the tennantite-sphalerite assemblage from the gold-polymetallic stage using the geothermometer suggested by Sack (Sack and Loucks, 1985). The data obtained showed that its formation temperature ranged from 111 to 379ºC (commonest 150-250 ºC) in different veins (Table 3).

Bi minerals

Bismuth reserves at the Berezovsk deposit are estimated as more than 1000 t (Ovchinnikov, 1998). In the sulphide-quartz veins, bismuth occurs in mineral forms or as an admixture in galena, tennantite-tetrahedrite and native gold. Bismuth minerals are represented by native bismuth, simple sulphides (bismuthinite), selenides (guanajuatite), sulphotellurides (tetradymite), and sulphobismuthites of Pb (cosalite), Pb–Cu (aikinite), Ag (matildite) and Cu (wittichenite, emplectite). The major part of bismuth is related to aikinite. Aikinite occurs as needle-like and prismatic crystals and its aggregates. Aikinite is often associated with galena II, matildite, gersdorffite, and native gold II. Chemical composition of some Bi minerals and various generations of chalcopyrite, sphalerite and galena is shown in Table 4.

4 FLUID INCLUSIONS

4.1 Fluid inclusion petrography

The study of fluid inclusions (FI) using the standard techniques has been carried out for the various generations of quartz, carbonate and sphalerite from the auriferous veins and for the quartz from the early quartz-tourmaline veins. Fluid inclusions with 20 to 100 μm in size, generally ellipsoidal, irregular or negative shape were revealed. The primary and secondary inclusions were identified according to the criteria of Roedder (1984). The widespread primary fluid inclusions are distributed along the growth zones or as random clusters within the quartz grains. The secondary fluid inclusions are less abundant and fill cracks or form the chain-like clusters intersecting the grain boundaries. The primary fluid inclusions are subdivided into three types by phase composition at room temperature: (I) three-phase aqueous-carbon dioxide fluid inclusions containing liquid water as well as liquid and gaseous CO_2; (II) mono-phase vapour CO_2-rich inclusions, sometimes with a thin liquid rim; (III) two-phase aqueous inclusions containing liquid H_2O + vapour H_2O. Type I and II fluid inclusions are localised in the same growth zone of minerals that suggests their contemporaneous trapping. Thus, minerals crystallised under conditions where two immiscible fluids coexisting in the system were products of H_2O-CO_2-NaCl fluid separation into two phases: substantially liquid and substantially gaseous.

4.2 Microthermometry

Individual inclusions have been studied using a microthermometric system consisting of LINKAM THMSG 600 chamber with 50× long-focus objective lens installed on BX-53 Olympus microscope, video camera and control computer. The accuracy of

temperature measurements is ±0.2°C within temperature interval from –60 to +60 °C and decreases at higher and lower temperatures. The composition of predominant salts in aqueous solutions was estimated from the melting temperature of eutectic (T_{eut}) (Borisenko, 1977; Crawford, 1981; Davis et al., 1990). The total concentration of salts in fluid inclusions has been estimated by the clathrate melting temperature and ice melting temperature based on NaCl–H_2O system experimental data (Bodnar and Vityk, 1994). Pressure was determined on the base of the intersection of isochore and isotherm (Kalyuzhny, 1982) for syngenetic FI of types I and II. Salinity, density and pressure were estimated using FLINCOR program (Brown, 1989). The measurements have been carried out for fluid inclusions assemblages with similar phase proportions in order to exclude the possible error due to the necking of the vacuoles after fluid heterogenisation (Roedder, 1984). The results of the microthermometric data measured for more than 250 fluid inclusions at the Berezovsk deposit are shown in Table 5 and are plotted in Figure 14.

Early quartz-tourmaline veins

Early quartz hosts two-phase fluid inclusions of type III. The inclusions contain fluid of complicated composition with eutectic temperatures (T_{eut}) from –44 to –49°C that is typical for Mg(Ca,K)-chloride solutions. Final ice melting temperatures ($T_{m(ice)}$) occur between –21° and –19°C, equivalent to salinities of 21.7 to 23.0 wt % NaCl equiv. The homogenisation temperature ranges within 195 – 220°C.

Ankerite-quartz stage

Fluid inclusions in the vein quartz and carbonate comprise type I and II inclusion assemblages. Type III of FI was recognised only in carbonate. Inclusions of type I exhibit uniform eutectic temperatures ranging from –34 to –30.1°C, indicating the dominance of Na^+ and Mg^{2+} cations. Fluid inclusions generally demonstrate a narrow CO_2 melting temperatures range ($T_{m(CO2)}$) from –57.2 to –56.7°C that is slightly below the CO_2 critical point of –56.6°C (i.e., near-pure CO_2 compositions), suggesting the presence of minor CH_4 and N_2 in the trapped fluid. The homogenisation of CO_2 ($T_{h(CO2)}$) into liquid occurred at 23 to 30.1°C. Melting temperatures of clathrate ($T_{m(clathrate)}$) are between 3.8 and 6.1°C, that is equivalent to salinities of 7.3 to 10.4 wt % NaCl equiv. The homogenisation temperature of FI ranges from 264 to 238°C. The density of the homogeneous fluid does not exceed 0.5–0.6 g/cm^3. Type II of FI contains high-density CO_2 with melting temperatures ($T_{m(CO2)}$) from –57.1 to –56.7°C and homogenises at 20

to 30°C. The salinity of the aqueous FI (III type) varies between 7.3 to 8.5 wt % NaCl equiv. The majority of the H_2O-CO_2-NaCl (type I) and CO_2-rich (type II) FI displays similar $T_{m(CO2)}$ and $T_{h(CO2)}$ that is a good additional evidence of their genetic link. The pressure estimated by syngenetic FIs is 489–566 bar.

Pyrite-quartz stage

Fluid inclusions of three types (I, II and III) were recognised in quartz from this stage. Type I of FI contains Na- and Mg-Na chloride solutions (T_{eut} from -28.1 to -36°C). The melting temperature of CO_2 ($T_{m(CO2)}$) varies from -63.4 to -57.9°C. This fact indicates the variable concentrations of N_2 and/or CH_4 within this inclusion type. Melting temperatures of clathrate ($T_{m(clathrate)}$) vary from 1.8 to 5.4°C, corresponding to the narrow salinity range from 8.6 to 13.4 wt % NaCl equiv. The homogenisation of CO_2 ($T_{h(CO2)}$) into liquid occurred at 0.8 to 26°C. Inclusions homogenised at temperature between 293 and 230°C. The density of the fluid was 0.5–0.7 g/cm^3. Type II of FI contains dense liquid CO_2 with $T_{m(CO2)}$ between –63.5 and –57.9°C, implying the presence of additional gases apart from CO_2. The majority of type II inclusions homogenises into the liquid phase ($T_{h(CO2)}$) from 1.0 and 25.4°C. The pressure estimated by syngenetic inclusions ranges 445–851 bar.

Gold-polymetallic stage

Fluid inclusions of I and II types were recognised in quartz and sphalerite from this stage. Aqueous-carbonic inclusions of I type show $T_{m(CO2)}$ between –58.5 and –56.7°C, indicating the presence of additional gas species; is $T_{h(CO2)}$ mainly from 1.5 to 22.7°C; and positive $T_{m(clathrate)}$ values between 0.3 and 6.0°C, corresponding to salinities from 7.5 to 15.3 wt % NaCl equiv. Homogenisation temperatures display a wide range between 301 and 210°C (FI in quartz) and from 233 to 200°C (FI in sphalerite). This inclusion type exhibits T_{eut} from –46 to –29.6°C, indicating the dominance of Mg^{2+} cations in chloride solution. Bulk densities range from 0.53 to 0.85 g/cm^3. Type II of FI contains dense liquid CO_2 that melts at temperatures from –58 to –56.7°C and homogenises at 5.0 to 25°C. The pressure calculated by syngenetic I and II types of FI is 607–1609 bar.

New obtained data complement our early studies (Bortnikov et al. 1998, Vikent'eva et al., 2000) and are consistent with previously received data showing the evolution of the PTX-parameters of ore-forming fluid. Additional fluid inclusion investigations by Baksheev et al. (2001), Konstantinov et al. (2002) and Garofalo et al. (2014). Baksheev

et al. (2001) demonstrated that the early scheelite-quartz veins were formed at 365-270°C and 3.5-1.5 kbar from solutions with salinity of 14.9 to 2.4 wt % NaCl equiv. and CO_2 concentration of 6.3 to 3.1 mole/kg of solution. The quartz of the late auriferous quartz-sulphide assemblages was crystallised at 335 to 255°C and 2.9 to 0.8 kbar from solutions with salinity of 9.0 to 2.0 wt % NaCl equiv. and CO_2 concentration of 5.3 to 3.1 mole/kg of solution. These data indicate the presence of high temperature and low-salinity fluids in the Berezovsk hydrothermal system. The difference of the this data from our results is explained by the fact that Baksheev et al. (2001) investigated samples from the deeper zones of the deposit (Fig.14). Konstantinov et al. (2002) showed that the sulphide-quartz veins were formed at 390-250°C and 1.8-0.4 kbar from solutions with salinity of 15.5 to 5 wt % NaCl equiv. Extremely low-salinity solutions (0.4 to 4.7 wt. % NaCl equiv.) at 202 to 295°C were obtained by Garofalo et al. (2014).

4.3 Ion and gas analyses

Ion chromatographic analyses revealed that Cl^- is the dominant ion in a fluid trapped in the fluid inclusions. Its content in the fluid released from the samples studied ranged from 0.04 to 1.07 mole/kg H_2O. Minor F^- (0.002 to 0.04 mole/kg H_2O, very rarely up to 0.96 mole/kg H_2O) and SO_4^{2-} (<0.002 to 0.008 mole/kg H_2O, very rarely up to 0.13 mole/kg H_2O) were also detected. The F/Cl ratio varies from 0.01 to 0.45 and 0.44 to 1.33 for the fluid inclusions in early and late quartz, respectively, indicating the increase of fluorine role during the mineral forming process.

Gas chromatography also showed that CO_2 was a major volatile component trapped in fluid inclusions. Its content in the fluid released from inclusions ranged from 2.3 to 31.7 mole/kg H_2O. CH_4 and N_2 are minor constituents. The N_2 and CH_4 contents lie within 0.01 to 0.16 mole/kg and <0,001 to 0.03 mole/kg, respectively (Fig. 13). The positive correlation between CO_2/CH_4 and CO_2/N_2 values for the hydrothermal solutions suggests that liquid-vapour separation occurred in the system (Sherlock et al., 1999). This is in good correspondence with an abundance of syngenetic fluid inclusions with dominance of CO_2 vapour resulted from fluid immiscibility (Bortnikov et al., 1998).

4.4 Laser Raman analysis

The V-rich fluid inclusions noted above were examined using laser Raman to investigate the possible presence of condensed gases. FI were analysed at the Saint Petersburg Resource Centre "Geomodel" (analyst V.N. Bocharov). The V-rich FI in quartz from pyrite-quartz and gold-polymetallic stages mainly contain CO_2 (100 mol.%,

14 FIs) whereas other gases (H_2, O_2, N_2, CH_4, H_2S) were not detected. In two inclusions in quartz from gold-polymetallic stage the admixture of CH_4 (1.2-1.6 mol. %) was detected in addition to CO_2 (98.8-98.4 mol. %).

5 STABLE ISOTOPES

Stable isotopes (H, O, C, and S) in minerals of the Berezovsk deposit have been discussed by (Bortnikov et al., 1997, 1998, 2001; Vikent'eva, 2000a), although an early study has documented a zonal distribution of sulphur isotopes in pyrite crystals (Igumnov et al., 1978). Baksheev et al. (2001) obtained data on the oxygen isotope fractionation between coexisting quartz and scheelite. The sulphur isotope composition of pyrite was studied by Kryazhev et al. (2011).

Stable isotopes in minerals from host metamorphic rocks, metasomatically altered host rocks and auriferous veins have been studied. Analyses for sulphur isotope composition of sulphides, oxygen and carbon isotope composition of carbonates, oxygen isotopes of quartz, oxygen and hydrogen isotope composition of silicates have been carried out. Samples were prepared using conventional magnetic and heavy liquid techniques. Estimation of purity was based on microscopic and X-ray powder diffraction study. Standard techniques for extraction and analyses were used as described by Kyzer (1987). Sulphides, carbonates and quartz were studied at IGEM Russian Academy of Sciences, silicates were analysed at the Department of Isotope Studies Scottish Universities Research and Reactor Centre.

5.1 Stable (H, O, C) isotopes in minerals from alteration halos

Stable isotopes in silicate and carbonate minerals from host rocks and from different zones of altered halos adjacent to quartz veins were studied. Three profiles through the altered basalt, gabbro and serpentinite metamorphosed to greenschist facies (that is apobasaltic, apogabbroic and aposerpentinitic alteration) were investigated.

5.1.1 D and O isotopes of silicates

The δD and $\delta^{18}O$ values in minerals from host rocks are in limits from –87 to –48‰ and +3.0 to +9.5‰, respectively (Tabl. 6). The δD and $\delta^{18}O$ values of minerals from metabasalt range from -58 to -48‰ and from +3.0 to +9.1‰ and decrease in the sequence: actinolite – chlorite – epidote. Actinolite from metabasalt is richer in ^{18}O

isotope by +2‰ in comparison to amphibole from gabbro. Their difference in δD values is significant: actinolite is depleted in deuterium by 29‰.

The δD and $\delta^{18}O$ values of silicates from altered rocks are within –43 to –63‰ and +6.4 to +11.0‰, respectively (Tabl. 6). A slight enrichment in heavy oxygen isotope of sericite and fuchsite relative to chlorite and amphibole is observed.

The obtained data show the uniformity of the $\delta^{18}O$ values measured for metamorphic minerals except epidote. On the contrary, δD values differ widely and appear to correlate with host rock composition. These data indicate that there was no significant perturbation in $\delta^{18}O$ values of minerals during metasomatic replacement of metamorphic rocks, while the deuterium isotopic composition of minerals was significantly changed.

5.1.2 C and O isotopes of carbonates

The $\delta^{18}O$ and $\delta^{13}C$ values of carbonate minerals from metamorphic rocks vary from +16.5 to +21.8‰ and from –14.2 to –3.2‰, respectively (Table 6, Fig. 15). Breunnerite from the aposerpentinitic listvenite is rich in heavy O and C isotopes ($\delta^{18}O$= +24.4 to +27.8‰, $\delta^{13}C$= –6.8 to –3.0‰). The $\delta^{18}O$ and $\delta^{13}C$ values of minerals from the apobasaltic listvenite are +16.6 to +26.6‰, and –5.4 to –11.8‰, respectively. Ankerite from the apogabbroic listvenites has the $\delta^{18}O$ and $\delta^{13}C$ values of +21.2±0.8‰ and –6.0±0.5‰, respectively. Breunnerite from these rocks has the $\delta^{18}O$ and $\delta^{13}C$ values equal to +16.0 and –8.0‰, respectively. Thus, the influence of the host rock composition on the $\delta^{13}C$ and $\delta^{18}O$ values in the carbonate minerals from altered rocks has been observed. The increase of degree of alteration rock (from unaltered rock to listvenite) corresponds to enrichment of carbonates of ^{16}O and ^{12}C isotopes.

5.2 Stable (O, C, S) isotopes of minerals from auriferous veins

5.2.1 C and O isotopes of carbonates

The $\delta^{18}O$ and $\delta^{13}C$ values of carbonates from auriferous veins range from +14.5 to +24.6‰ and –19.4 to –2.8‰, respectively (Fig. 15). The variations are wider than those, namely, of +18.1 to +22.7‰ and –8.4 to –6.1‰ reported previously for oxygen and carbon, respectively (Bortnikov et al., 1997). Differences in $\delta^{13}C$ values of vein carbonates located in different dykes are shown in Fig. 15. Late vein carbonates are richer in ^{12}C isotope: $\delta^{13}C$ values change from –10.7 to –19.4‰. Outer zones of carbonate crystals as well as carbonates from the central parts of veins are also rich in

a light isotope of carbon. The $\delta^{13}C$ values for carbonates in association with tennantite-tetrahedrite minerals are from –2.8 to –5.2‰. The weakly-pronounced positive correlation of $\delta^{18}O$ and $\delta^{13}C$ values in carbonates was found. The most of the $\delta^{18}O$ and $\delta^{13}C$ values of carbonate minerals from auriferous veins coincides with the range of values obtained for carbonates from the altered rocks. Kryazhev et al. (2011) reported the $\delta^{18}O$ values for the late Fe-calcite of +9.7 to +13.8‰ that is lower than our data.

5.2.2 Oxygen isotopes of quartz and scheelite

An oxygen isotope composition of quartz and scheelite from pyrite-quartz stage and of quartz from gold-polymetallic stage was studied. The $\delta^{18}O$ values of early quartz and scheelite are of +10.4 to +11.4‰ and +9.2 to +14.1‰, respectively. Baksheev et al. (2001) found that $\delta^{18}O_{quartz}$ = +9.1 to +16.0‰ and $\delta^{18}O_{scheelite}$ = +2.0 to +6.6‰. The $\delta^{18}O$ values of late quartz from gold-polymetallic stage range from +5.6 to +17.2‰. Obviously, the late quartz is rich in light oxygen isotope relatively to the early quartz. ^{18}O-enricment of varieties of late quartz in the order milky quartz – translucent quartz – quartz crystal was found. These data extend the preliminary conclusion that the $\delta^{18}O$ values of quartz from auriferous veins exhibit narrow range of +9.7 to +11.7‰ (Bortnikov et al., 1998). The variations in the $\delta^{18}O$ values of quartz from auriferous veins hosted by different dyke are observed. Milky quartz from the Vtoropavlovskaya dyke ($\delta^{18}O$ = +10.6 to +15‰), Ilyinskaya dyke ($\delta^{18}O$ = +11.2 to +16.3‰), Soimonovskaya dyke ($\delta^{18}O$ = +12.6 to +17.2‰) displays relatively uniform $\delta^{18}O$ values averaged at +13.3‰. Quartz from the Soedinennaya dyke is rich in ^{16}O ($\delta^{18}O$ = +5.6 to +7.3‰). Oxygen isotope composition of quartz from sulphide-quartz veins of the Shartash massif ($\delta^{18}O$ = +9.7 to+11.2‰) is almost identical to the values obtained for early quartz of ladder veins.

5.2.3 Sulphur isotopes of sulphides

Sulphur isotope composition of pyrite, chalcopyrite, sphalerite, galena and tennantite from auriferous quartz veins and sulphide disseminated in adjacent wall rocks as well as sulphides from the veins hosted by the Shartash massif was studied. The $\delta^{34}S$ values obtained (about 150 analyses) ranges from –3.5 to +13.7‰ (Fig. 16). The $\delta^{34}S$ values of pyrite from beresites and auriferous veins are between +2.6 and +10.9‰ and +2.1 and +13.7‰, respectively. Some large pyrite crystals display a pronounced zoning in the sulphur isotopic composition due to a ^{32}S-enrichment of outer zones

(Bortnikov et al., 1997). The range of the $\delta^{34}S$ values found for chalcopyrite is from +4.6 to +12.7‰. Galena and tennantite show $\delta^{34}S$ compositions between –3.5 and +9.8‰ and –3.2 to +11.6‰, respectively. These data suggest an enrichment of the late sulphides in the light ^{32}S isotope (Fig. 16). The sulphur isotope compositions of pyrite from auriferous veins hosted by different dykes are as follows: +4.1 to +11.5‰ from the Ilyinskaya dyke, +2.1 to +13.7‰ from the Vtoropavlovskaya dyke, +2.6 to +10.1‰ from the Soimonovskaya dyke, +5.9 to +13.7‰ from the Soedinennaya dyke, and +9.2 to +12.4 from the Elizavetinskaya dyke. Therefore, the differences of the $\delta^{34}S$ values of the sulphides from the ladder veins located in the various dykes appear to be insignificant. Sulphides from sulphide-quartz veins occurred within the Shartash granitoid massif show similar composition (+3.4 to +8.0‰ for pyrite, –3.7 to +2.8‰ for galena, +4.6‰ for tennantite, and +4.9‰ for sphalerite) to minerals from auriferous veins.

Kryazhev et al. (2011) found two isotopic varieties of pyrite with modal $\delta^{34}S$ values close to + 1.5‰ and to +8.5‰. Konstantinov et al. (2002) reported the $\delta^{34}S$ values of +1.6 to +3.6‰ and of +7.5 to +10.5‰ for early and late pyrite, respectively, and of –0.4 to +3.3‰ for sulphides from the sulphide-quartz veins in the Shartash massif. The authors revealed zonal variation in $\delta^{34}S$ values of pyrite: the $\delta^{34}S$ values increase from weakly altered granite-porphyry to veins and increase from cores to inner zones of crystals. The ^{32}S-enrichment of sulphides from Vtoropavlovskaya dyke with increasing of depth and to the southern flank towards the Shartash massif was found (Konstantinov et al., 2002; Kryazhev et al., 2011). Pyrite, disseminated in the host volcanic-sedimentary rocks, yields a wide range of $\delta^{34}S$ values of –15.8 to +1.3‰ (Konstantinov et al., 2002), and is mainly richer in light ^{32}S isotope than sulphides from auriferous veins.

5.3 Isotope composition of the hydrothermal fluid and fluid reservoirs

The results of C, O, H and S isotope measurements for minerals combined with fractionation factors and fluid inclusion homogenisation data were used to calculate the isotopic composition of hydrothermal fluid according to the equations of fractionation in hydrothermal systems (O'Neil and Taylor, 1969; Wenner and Taylor, 1971; Ohmoto, 1972; Ohmoto and Rye, 1979; Matsuhisa et al., 1979; Wesolowskii and Ohmoto, 1986; Zhou and Dobs, 1995; Ojala et al., 1995; Li and Liu, 2006).

The quartz+sericite+carbonate+pyrite assemblage in altered host rocks indicates that the mineral-forming fluid was near-neutral to slightly acid at 200 to 300°C (Zaraisky, 1989) and was buffered by its reactions with host rocks. Fluid inclusion data and mineral

association suggest that the fluid redox state was below SO_2/H_2S boundary (sulphate minerals are absent) and above CO_2/CH_4 equilibrium (the CH_4 content in fluid is minor). The uniform FeS content in sphalerite can indicate insignificant variation of the fluid redox state. Thus, the dominant form of carbon was H_2CO_3 (or CO_2) that implies $\delta^{13}C_{H2CO3}=\delta^{13}C_{CO2}=\delta^{13}C_{fluid}$. Also, H_2S was the dominant sulphur species in the fluid ($\delta^{34}S_{H2S}=\delta^{34}S_{fluid}$) assuming the depositional temperatures of 200 to 300°C and depositional parameters did not have a substantial effect on the variations in the $\delta^{34}S$ values of the sulphides.

5.3.1 Isotopic composition of fluid from alteration halos

The $\delta^{18}O$ and δD values of fluid calculated in equilibrium with metamorphic minerals at 350°C vary from +2.0 to +10.2‰ and –12 to –34‰, respectively (Fig. 17). The calculated values fall partly in or out but close to $\delta^{18}O$–δD box of typical metamorphic waters (Sheppard, 1986).

The $\delta^{18}O$ and δD values of +5.2 to +8.1‰ and –39 to –63‰ were estimated for the fluid responsible for the alteration process assuming formation temperature of 275°C (Fig. 17). The $\delta^{18}O$ value of fluid equilibrated with chlorite and as well as with white mica (sericite and muscovite) remains nearly the same (+6.0±2‰) across the apobasaltic alteration halo, while the δD values evolve from about –40 to –60‰. This trend was revealed for fluid equilibrated with fuchsite from apogabbroic and aposerpentinitic metasomatites. It seems clear that there is dependence between δD values of micas from listvenites and δD values of minerals from host rocks: when an initial mineral is lighter in hydrogen isotope, newly-formed mica is also lighter. These data indicate that hydrogen isotope composition of fluid depends on hydrogen isotope composition of minerals in host rocks and from alteration degree of host rocks. Possibly, the observed change in the δD values reflects the hydrogen isotope evolution of the fluid responsible for the formation of alteration halo. Therefore, the isotopic composition of the fluid equilibrated with mica from the inner zones of the alteration halos is proposed to be the closest to the isotopic composition of a reservoir. Under this condition the $\delta^{18}O$ and δD values of the fluid are estimated at +6.5±1.5‰ and –60 to –40‰, respectively. The δD and $\delta^{18}O$ values of the fluid formed alteration halos fall in both boxes typical for magmatic water and metamorphic water (Fig. 17). However, fluid in equilibrium with the metamorphic minerals of host rock is rich in the $\delta^{18}O$ relative to the fluid in equilibrium with metasomatites. It is evident that the δD and $\delta^{18}O$ values calculated for mineral-

forming fluid are different from the values obtained for metamorphic fluid that allows to suppose that the hypothesis on a contribution of magmatic fluid seems to be favourable.

The $\delta^{13}C_{CO2}$ values of the fluid altering the host rocks at 275°C vary from –10.1 to –4.7‰, from –6.3 to –3.1‰ and from –5.1 to –0.4 for apobasaltic, apogabbroic and aposerpentinitic metasomatites, respectively. The average $\delta^{13}C_{CO2}$ of the fluid equilibrated with carbonates from the inner zones of metasomatic halos is –5.3‰ and falls within the interval typical for magma-derived fluids (–7 to –2‰; Ohmoto, 1986).

5.3.2 Isotopic composition of ore-forming fluid

Oxygen isotopes

The oxygen isotopic composition of fluids was calculated in accordance with equations of fractionation in hydrothermal systems using measured $\delta^{18}O$ in quartz and scheelite and homogenisation temperature of fluid inclusions.

The calculated $\delta^{18}O$ values of the fluid forming the mineral assemblages of pyrite-quartz stage at 280°C are +3.3±0.5‰ and from +10.5 to +15.4‰ in equilibrium with quartz and scheelite, respectively. These data indicate isotopic disequilibrium between these minerals. Microscopic investigations of the samples showed an evidence for partial recrystallisation of minerals. Abundant populations of secondary fluid inclusions in scheelite are an evidence that this mineral has been recrystallised. Quartz of the gold-polymetallic stage was formed from the fluid, where $\delta^{18}O$ commonly varied from +3.0 to +9.6‰ except to 5 samples with values equal to -2 to -0.3‰. Low $\delta^{18}O$ values were estimated for the samples from the flank of the deposit.

The average $\delta^{18}O_{H2O}$ for the mineral-forming fluid coexisting with native gold mineral assemblages is +6.2‰, that is close to above estimated $\delta^{18}O_{H2O}$ of +5.2 to +8.1‰ (averaged at +6.5‰) on the basis of oxygen isotope composition for silicate minerals from the alteration halo. These data support the involvement of magmatic water in the formation of auriferous veins of the Berezovsk deposit. The deposition of isotopically light quartz in veins can be a result of an input of the ^{18}O-isotope depleted heated meteoric water. An isotopic shift of the fluid due to fluid immiscibility can also be responsible for this phenomenon, because the phase separation demonstrated by the fluid inclusion study may contribute to the depletion in the ^{18}O isotope in the residual fluid (Bowers, 1991).

Baksheev et al. (2001) found that calculated oxygen isotopic composition of the fluid equilibrated with quartz and scheelite at temperature of 315±35°C were +1.5 to +10.3‰ and +4.0 to +8.7‰, respectively, the authors suggested that the fluid was

magmatic in origin during the early mineral-forming process. The mineral-forming fluid in equilibrium with late Fe-calcite was enriched with ^{16}O (Kryazhev et al., 2011); the $\delta^{18}O_{H2O}$ varies from +2.2 to +6.3‰ at 250±30°C.

Carbon isotopes

Values of $\delta^{13}C$ for fluids coexisting with early carbonates from the ankerite-quartz and pyrite-quartz stages change from –1.7 to –7.7‰ (280-300°C) that coincides with values $\delta^{13}C_{CO2}$ estimated by carbonates of metasomatites. Fluid coexisting with late carbonates is ^{12}C-enriched ($\delta^{13}C_{CO2}$ varies from –9.5 to –18.5‰).

The $\delta^{13}C_{CO2}$ values calculated for mineral-forming fluid equilibrated with early vein carbonates may indicate an input of magma- or mantle-derived carbon. Shift toward to ^{12}C-enrichment can be caused by formation of abundant carbonates in alteration halos adjacent to veins and in ankerite-quartz stage, accompanying by CO_2-depletion in the fluid due its incorporation in the carbonate minerals. This process can lead to an enrichment of the fluid with light isotope (Zhou and Dobs, 1995). An isotopic shift of the fluid due to removal of the carbon dioxide in the mineral phase is estimated as 8‰ for open system (Bychkov, 2012); carbonates precipitated from such residual fluid will be depleted in the heavy carbon isotope.

The $\delta^{13}C$ values for CO_2 generated at the oxidation-reduction reactions of the organic carbon range from –10 to –35‰ (Ohmoto and Rye, 1979). Thus, a presence of carbonate minerals equilibrated with CO_2 having $\delta^{13}C$ of –10.1 to –17.6‰ can be an evidence for the involvement of organic carbon in the Berezovsk hydrothermal system. This carbon can be derived from carbonaceous metasidementary rocks with graptolite remnants that are widespread at north-eastern exocontact of the Shartash granite massif.

The $\delta^{13}C$ values from CO_2 extracted from fluid inclusions in early and late carbonates are −7±1‰ (Kryazhev et al. 2011). Such values are typical for magma-derived CO_2 (Ohmoto, 1986; Jia et al., 2001), therefore the contribution of the magmatic fluid during deposition of ore assemblages can be assumed. CO_2 derived during decarbonation and dehydration reactions is rich in ^{13}C (Faure, 1986). Our data suggest that the input of the fluid of metamorphic origin into hydrothermal system was insignificant.

Sulphur isotopes

The $\delta^{34}S_{H2S}$ values of the fluid responsible for the formation of pyrite in the alteration halo are limited from +1.4 to +9.7‰ at 275°C. These values of fluid equilibrated with pyrite and chalcopyrite from auriferous veins vary from +1.4 to +12.5‰ and +4.8 to +12.9‰, respectively. The sulphur isotope composition of the fluid deposited during the late gold-sulphide mineralisation was estimated on the data on $\delta^{34}S$ values obtained only for galena because there is no experimentally or theoretically derived fractionation factor for tennantite-tetrahedrite minerals. The $\delta^{34}S_{H2S}$ value of the fluid responsible for the formation of this mineral ranges from –1.6 to +11.7‰. The ^{32}S-enrichment of fluid equilibrated with late sulphides was revealed. The ^{32}S-enrichment of late portions of the fluid corresponds to isotopic zoning of the large pyrite crystals with depletion of outer zones in ^{34}S (Bortnikov et al., 1997).

Two processes could be responsible for this phenomenon: (1) mixing of the early fluid with the ^{34}S-depleted fluid, and (2) the fluid immiscibility resulting in enrichment in ^{32}S isotope of H_2S in a residual fluid (Ohmoto, 1986; McKibben and Eldridge 1991). Fluid immiscibility accompanied by removal of reduced gas species from primary ore fluid leads to enrichment of the residual fluid with ^{32}S light isotope and reflected in $\delta^{34}S$ depletion of sulphides. This resulted from the faster rate of the H_2 loss relative to the H_2S escape that leads to the H_2S_{aq} oxidation (Bowers, 1991; Brown, 1989). The shift in the $\delta^{34}S_{H2S}$ value is controlled by temperature and the fraction of H_2S escaped and can be estimated using the Rayleigh equation: $\delta_f - \delta_i = (1000 + \delta_i)(1 - F^{\alpha-1})$, where δ_i и δ_f – initial and final isotope ratios, respectively, in the fluid, F – mole fraction of a component in the residual fluid, and α - isotope fractional factor (White, 2015). Oxidation of 10% and 30% of H_2S at 350°C shifts the sulphur isotope composition in the residual fluid by –2‰ and –6.8‰, respectively. This estimation clearly shows that this phenomenon can be responsible for the evolution of fluid isotope composition in the Berezovsk hydrothermal system. This mechanism seems to be preferable because the fluid immiscibility was documented by the fluid inclusion study.

Estimated $\delta^{34}S_{H2S}$ values are significant wider than the typical values for a sulphur derived from magmatic sources ($\delta^{34}S$ is between –3.0 and +7.0‰, Ohmoto, 1986) due to the enrichment of the heavy ^{34}S isotope. The value of $\delta^{34}S \approx 13$‰ for the fluid suggests that sulphur was partly introduced from sedimentary rocks. However, pyrite disseminated in the host rocks of Berezovsk ore field is mainly ^{32}S-enrichment (Konstantinov et al., 2002). In addition, the enrichment in heavy S isotope up to +17‰ of granitic rocks due to an assimilation of sedimentary rocks has been found (Ohmoto

1986; Poulson et al. 1991). Taking into account this fact, we suggest that the sulphur can be magmatic in origin. However, we could not completely exclude that some part of S depleted in ^{34}S was extracted from the host mafic-ultramafic rocks.

6 DISCUSSION

The origin of ore-forming fluids is the most discussed issue for the Berezovsk gold deposit. Magmatic and metamorphic fluids often do not differ in composition and PT parameters. The typical metamorphic fluid is rich in CO_2 and has relatively low salinity (e.g., Groves et al., 1998; Yardley and Bodnar, 2014), whereas metamorphic fluids in calcareous rocks have salinity of up to 20-25 wt % NaCl equv. (Pirajno, 2009). Salinity of magmatic hydrothermal fluids depends on the relative proportions of H_2O, Cl^- and CO_2 in the magmas (Baker, 2002). Both magmatic and metamorphic fluids have similarly wide ranges of temperature and pressure data. On this basis, the comprehensive geological, mineralogical, fluid inclusion and stable isotope study has been undertaken for the genetic reconstruction of the Berezovsk hydrothermal system. No single characteristic is diagnostic, but a suite of features is the most effective to provide evidence of the origin.

6.1 EVIDENCE OF FLUID SOURCE

Geological evidence

The Berezovsk deposit is spatially related to the Shartash granite massif. The gold-bearing veins hosted in the granitoid dykes in the apical part of the Shartash granite massif, as well as mineral and metal zoning relative to granite massif, imply a genetic connection between gold ores and granitic pluton. Geochemical similarity and the same age of granitoids from the dykes and the massif allow us to consider the dykes as derivatives from the deep parts of the Shartash granite massif (Sazonov et al., 1999). This massif together with the Verkhiset batolith and a few smaller mainly granitic intrusions compose the Verkhiset magmatic area, being continuously formed from the Famennian until the Kungurian (Pribavkin and Pushkarev, 2011; Fershtater, 2013), which implies a prolonged magmatic activity in the vicinity of the Berezovsk deposit. This factor favoured for the formation of the large gold-ore system (Bortnikov et al., 1997; Sazonov et al., 2001; Fershtater et al., 2010). The $^{206}Pb/^{238}U$ age of Shartash granite massif of 302±2 Ma (Fershtater et al., 2010), the $^{206}Pb/^{238}U$ age of Au-vein-hosted granite-porphyry dyke of 305±7 Ma (Pribavkin and Pushkarev, 2011) and $^{40}Ar/^{39}Ar$ age of lamprophyre dyke crossing the sulphide-quartz veins of 284.4±3.6 Ma

(Pribavkin et al., 2007) determine the probable age of the gold mineralisation as ca. 300 Ma.

Overprinting on metamorphic minerals and igneous rocks by the low-temperature quartz-sericite-carbonate-pyrite mineral assemblage clearly indicates that the gold mineralisation at the Berezovsk deposit was formed after the peak of regional greenschist facies metamorphism and emplacement of the granitoid rocks and dyke series of the Shartash massif.

The main feature of the granitic rocks of the Shartash massif is its generation from H_2O-rich (3 to 8 wt % H_2O) magmas (Fershtater et al., 2013). The granitic magma was also rich in volatiles such as Cl, F and SO_3 as follows from the study of apatite from granites of the Shartash massif and granite-porphyry dykes of the Berezovsk deposit (Konovalova et al., 2012). This mineral contains from 0.26 to 1.08 wt % SO_3. An enrichment of sulphur in the magmatic system increases mobilisation and transfer of gold by supercritical Cl-bearing fluid: the partition coefficient increases from 2.0 to 4–12 (Gorbachev et al., 2007). The Shartash pluton features, such as porphyritic textures, aplite and pegmatite dykes, indicate a magmatic-hydrothermal origin of the fluid.

Mineralogical evidence

The scheelite-bearing quartz veins with gumbeite halo occurring around the Shartash massif dip at a low angle under the Berezovsk deposit. Auriferous sulphide-quartz veins accompanied by beresite-listvenite are distal from the massif's roof (Fig.19).

The change of mineral assemblages correlates with stratigraphic level and distance from the Shartash pluton. Magnetite and hematite are common in veins on the southern flank of the deposit, whereas pyrite and ankerite are abundant on the northern flank (Samartsev et al., 1973). The gold-polymetallic mineralisation is most widespread in the central part of the deposit, where the most productive veins are located. Sulphide-quartz veins with early Au-free and Au-poor assemblages (ankerite-quartz, rarely pyrite-quartz stages) are abundant on the flanks of the deposit. The lower boundary of the productive parageneses is approximately parallel to the surface of the Shartash granite massif. Vertical zoning is similar to the lateral zoning from the centre to the flanks of the deposit (Konstantinov et al., 2002). Chemical composition of native gold, sphalerite and tennantite-tetrahedrite minerals clearly indicates their significant variations in the ore field, which can be caused by the evolution of fluid composition or variations of physical and chemical conditions of crystallisation (Vikent'eva, 2000b). The fineness of native

gold decreases from the early to the late generations. The fineness of the early native gold decreases with the depth, whereas the fineness of the late native gold increases in this direction. Significant positive Ag-Sb correlation in the studied tennantite-tetrahedrite minerals may be a result of precipitation from hydrothermal solutions that were depleted mostly in As and Cu during the crystallisation. Such evolutionary trend could be attributed to a fractional crystallisation mechanism, causing the deposition of tennantite near the fluid source (Hackbarth and Putterson, 1984).

Zonal distribution of ore types (W and Au ore), altered rocks (gumbeite and beresite) and mineral assemblages as well as spatial variations of mineral chemistry at the Berezovsk deposit confirmed presence of mineral and metal zoning relative to the roof of the Shartash granite massif. The compositional zoning can be explained by the fluid evolution and the change of physical-chemical conditions of mineral formation relative to the fluid source that gives an additional argument for the significant contribution of magmatic fluid. The ores of the deposit were formed in four stages. The areal distribution of mineral assemblage of each stage is shifted to the north along the gentle roof of the granite massif. Smirnov (1982) believed that such zoning, named "pulsation zoning", was formed by the displacement of the focus of hydrothermal fluids flow along the gentle roof of the cooling intrusive. The input of new portions of fluid results in significant differences in mineral composition of stages that could not be explained only by the PT-evolution of the fluid. The multistage ore-forming process is more specific for hydrothermal system relative to magmatic source.

The ore mineral composition of the Berezovsk deposit, namely Bi and Te minerals, is a common characteristic of gold deposits in or close to plutons (Newberry et al., 1995). In addition to Au, Ag, Bi and W, these ores also contain subeconomic concentration of Cu (0.01-0.07%), Pb (0.07-0.5%) and Zn (0.04-0.06%). Therefore the Berezovsk deposit may be referred to as a gold-plus magmatic-hydrothermal deposit, in contrast to gold-only (orogenic) deposits with predominant metamorphic source (Tomkins, 2013).

Fluid inclusion evidence

The homogenisation temperatures, measured for the associations of fluid inclusion types I and II with similar relative amounts of phases, correspond to the two-phase liquid-vapour equilibrium curve in the H_2O–CO_2–NaCl system (Bowers and Helgeson, 1983). The values obtained for such heterogenic aqueous-carbonic fluid may be considered as real temperatures of mineral deposition, because pressure correction is

not required in this case (Roedder, 1984). The fluid inclusion study indicates formation of gold mineralisation at the Berezovsk deposit at 301 to 230°C and 0.3 to 2.3 kbar (mostly 0.5 to 1.2 kbar) from the H_2O-CO_2-NaCl fluid with salinity of 7.3 to 18.2 wt % NaCl equiv., that was separated into H_2O-CO_2-NaCl and CO_2-rich fluids due to the temperature and/or pressure drop at the deposition site. The abundance of carbonates in alteration as well as in the ore assemblages corresponds to infiltration of CO_2-rich hydrothermal fluid. Carbonate deposition results in substantial decrease of X_{CO2} in the fluid. High pressure values, obtained for the fluid coexisting with the gold-polymetallic assemblages and pointed in (Baksheev et al., 2001), suggest the overpressured formation conditions (Sibson et al., 1988; Yardley et al., 2000; Cox, 2016). The fluid pressure is relatively low during fluid flow through open fractures, and it increases as a result of partial to complete sealing of fractures by precipitation of hydrothermal minerals. The positive correlation between pressure and temperature was found. Baksheev et al. (2001) indicated similar trend between pressure and CO_2 concentration in the fluid. The mineral formation temperature decreases from early to late mineral assemblages within a stage, whereas a slight increase of temperature in late stages is observed as result of the input of new solution portion.

Salinity is not a distinguishable feature of the fluid source, but the metamorphic fluids generally have low salinity (3-7 wt % NaCl equv., Groves et al., 1998; Goldfarb et al., 1998) in contrast to the magmatic fluids (5-40 wt % NaCl equv, Baker, 2002). Calcareous rocks or buried brines in host rock undergoing metamorphism could be responsible for high salinity of metamorphic fluids (Yardley and Bodnar, 2014). However, host-rock lithology and oxygen isotope composition of the fluid demonstrate that these reasons are not applicable to the Berezovsk deposit. The increase of salinity as well as extension of salinity ranges from early to late stage of mineralisation was determined. This fact is consistent with fluid immiscibility accompanied by increase in NaCl content in residual fluid (Bowers and Helgeson, 1983).

Fluids responsible for the origin of the productive assemblages are rich in Au, As, Sb and contain Se, Mn, Cu, Ag and Bi according to ICP-MS analyses of aqueous extracts (Baksheev et al., 2001). The input of Sn, Mo and B during the beresitisation (Sazonov, 1975) and Cu-, Sb-, As- and Bi-enrichment of solutions are significant markers of the magmatic volatile contribution. In addition, K/Rb for fluid, calculated according to the data of Baksheev et al. (2001), range from 309 to 212, which is typical for magmatogenic processes (Shaw, 1968; Kerrich and Fryer, 1988), and tend to decrease with depth.

Isotopic evidence

Isotopic composition of hydrothermal fluid (see section 5.3 above) indicates the significant contribution of the magmatic fluid to the Berezovsk hydrothermal system. Evolution of isotopic composition of the fluid could be explained by phase separation of fluid predominantly of magmatic origin. This process led to enrichment of residual fluid by the light isotopes of oxygen and sulphur (Ohmoto, 1986; Bowers, 1991; McKibben and Eldridge, 1991). Formation of carbonates in the alteration halo and in the ore veins is accompanied by enrichment of the residual fluid with light carbon isotope (Zbou and Dobs, 1995; Bychkov, 2012). The $\delta^{13}C$ values of the fluid extracted from the fluid inclusions (−7±1‰, Kryazhev et al., 2011) are typical for magma-derived CO_2 (Ohmoto, 1986; Jia et al., 2001). Similarity of isotopic compositions of fluid, coexisting with the carbonate minerals from the altered rocks and the auriferous veins, indicates their single source. The values of fluid isotopic composition point to the time and spatial isotopic evolution. The ore-forming fluid is rich in light ^{16}O isotope on the flanks as compared to the central part of the deposit. This fact indicates the upward flow of fluid probably of magmatic origin in the central part of the deposit and its mixing with heated meteoric waters on the flanks (Vikent'eva, 2000a; Konstantinov et al., 2002).

6.2 MODEL OF THE BEREZOVSK HYDROTHERMAL SYSTEM

The granitoid dykes were intruded at the final stage of the Shartash massif emplacement (Rapoport et al., 1994). The compressional stress was vertical, while vectors of the maximal and intermediate tensions were approximately oriented east-west (in the present-day coordinates) and north-south, respectively (Fig.20). This stress state caused the opening of north-south faults above an apical zone of the massif. The faults were channels for emplacement of subvertical and steeply-dipping to the west granite-porphyry and plagiogranite-porphyry dykes. Modification of the deformational patterns by several east-west-oriented compressional events and, partly, sinistral north-south strike-slip motions led to the brittle deformation in the dykes. The compressional stress was oriented in the east-southeast direction, while the tension was in north-northeast direction. Such stress orientation was favourable for a generation of subvertical south-dipping shear fracture system and steeply-dipping to the south extension fissures. The supercritical fluid, exsolved during the granite massif crystallisation, migrated into colder host rock, penetrating along the systems of shear and extension fractures. The phase separation and loss of volatiles resulting from

disequilibrium between host rocks and ascending H_2O-CO_2-CH_4-NaCl fluid led to fluid-rock interaction and mineral deposition within the open shear and extensional fractures (Fig. 21).

Sulphide-quartz veins were formed in four stages: ankerite-quartz, pyrite-quartz, gold-polymetallic and carbonate. Brittle deformations, developed most intensely in the steeply-dipping north-south-striking dykes, produced the most economically important veins in these zones. The fluid/rock interaction caused metasomatic alteration of host rock accompanied by input of CO_2, K, S, loss of Na and Cr, Mg, Ca redistribution within the alteration halo (Sazonov, 1984). Beresitisation (325-260°C, 1.8-0.6 kbar) resulted in formation of quartz or carbonate veins (ankerite-quartz stage). At reducing acidity of solutions, the minerals of pyrite-quartz and gold-polymetallic stages were crystallised (285-150°C, 1.2-0.3 kbar). Pressure estimates (assuming lithostatic overburden) correspond to depths of 3 to 4.5 km. At the final stage of the process, calcite and dolomite were precipitated from the residual neutral solutions (160-80°C, 0.2-0.1 kbar). Fluid pressure evidently corresponded to hydrostatic pressure at the time of their formation. Based on this data, the palaeoreconstruction of the Berezovsk ore field for the end of the Carboniferous period was proposed (Fig. 22). Large native gold was formed when temperature falls from 260 to 80°C at constant pressure (0.3±0.05 kbar) according to carbonate geothermobarometry (Murzin et al., 1987). Large aggregation of native gold presumably formed during pumping of a large volume of gold-bearing solutions through a narrow zone of open extension fractures. The deposition of early sulphides in the veins could explain concentration of large native gold in the pockets.

The rock lithology was critical for localisation of the gold-sulphide-quartz veins. The most economically important high-grade ladder veins occur in the competent (brittle and elastic) granitoid rocks, where the dykes crosscut the relatively incompetent and ductile rocks, such as serpentinite, quartz-chlorite schist, siltstone, etc. The “krassyk” veins occurring mainly in serpentinite and metabasalt inherited reactivated ancient east-west-trending faults. Thus, the host rock sequence, consisting of interbeded volcano-sedimentary rocks and lens-like serpentinite bodies with different physical properties, was favourable for the fluid trapping at the petrophysical barrier. Overlapping serpentinised ultramafic rocks of the Pyshma-Berezovsk massif were also important as a barrier for the hydrothermal fluid flow. Fluid migration through the host rock with contrast physical properties induced the change in fluid redox state that formed the geochemical barrier for the deposition of ore components.

6.3 COMPARISON WITH IRGD AND OROGENIC DEPOSITS

The Berezovsk granitoid dyke-hosted gold deposit was considered by Russian geologists for a long time as a typical representative of the mesozonal gold-quartz deposits, spatially and genetically related to granitoid magmatism and formed at mid-crustal depth (Petrovskaya, 1972; Borodaevskaya, Rozhkov, 1974). This group of gold deposits may be referred to Lindgren's mesothermal deposits, for which a genetic connection between gold ores and granitic plutons was determined (Lindgren, 1933; Emmons, 1937).

The term "*intrusion-related gold deposits*" was introduced by Sillitoe (1991) for deposits in intrusion-related environment and included six classes: porphyry, skarn, intrusion-hosted, carbonate-replacement, breccia and vein. Sillitoe (1991) pointed out that intrusion-related gold deposits are genetically linked with I-type magmatism and suggested that many sedimentary and metamorphic terrain-hosted mesothermal deposits may be product of magmatic rather than metamorphic fluid. Later Newberry et al. (1995) proposed the term "*plutonic-hosted gold deposits*", emphasizing Bi and Te enrichments, and McCoy et al. (1997) applied the term "*plutonic related gold deposits*" indicating the magmatic fluid evolution and their differences from porphyry deposits. The nature of associated magma (Sillitoe and Thompson, 1998) as well as location within W-Sn provinces, Bi-Te-As-Mo-Sb metal association and genetic link with reduced granitic intrusion (Thompson et al., 1999; Thompson and Newberry, 2000) were taken into account. Lang et al. (2000) proposed the term "*intrusion-related gold system*" for such deposits, emphasizing variety of gold deposit styles within this class of deposits. Later, intrusion-related deposits were distinguished separately from epizonal and shear hosted deposits (Hart et al., 2002; Hart, 2005, 2007).

In recent years, emplacement of the Shartash granitoids, being the late phase of GTGG series, is discussed as partly synchronous with the continent/continent collision (Bortnikov, Vikentyev, 2013; Puchkov, 2017). This fact, as well as location of vein-hosted dykes in greenschist-metamorphosed host rocks, allowed some researchers to classify Berezovsk as an orogenic deposit (Goldfarb et al., 2005; Herrington et al., 2005).

The term "*orogenic"* gold deposits was originally suggested by Bohlke (1982) but it was widely introduced by Groves et al. (1998) "to replace 'mesothermal' and other descriptors for this deposit type". Orogenic gold deposits, usually located in or close to shear-zone, were formed during or immediately after compressional deformation and regional metamorphism from the fluids lacking any direct connection to intrusive rocks

(e.g., Phillips and Powell, 1993; Goldfarb et al., 1998; Groves et al., 1998; Groves et al., 2003; Goldfarb et al., 2005; Kerrich et al., 2005). There are many similarities between orogenic and intrusion-related gold deposits (Sillitoe and Thompson, 1998; Hart and Goldfarb, 2005). For this reason some gold deposits, especially those closely associated to granitoid intrusions, have been classified both as orogenic and as intrusion-related clans (De Boorder, 2012).

Distinguishing features of orogenic and intrusion-related deposits in comparison with the Berezovsk gold deposit are shown in Table 7.

CONCLUSIONS

This study proves a multiple source of the ore-forming fluids in the Berezovsk hydrothermal system. On the basis of geological, mineralogical, fluid inclusion and isotopic data, a predominantly magmatic source is proposed for hydrothermal fluid. The magmatic fluid evolved during its ascent and phase separation and mixing with fluid, derived from the host rock decarbonation and dehydration, and with meteoric water. As a consequence, the Berezovsk gold deposit is not only spatially, but also genetically related to the Late Carboniferous I-type Shartash granite massif. The Berezovsk deposit can be undoubtedly considered as intrusion-related gold deposit but not as orogenic gold deposit. This is supported by the mineral, metal and isotopic zoning, isotopic composition of minerals, as well as pluton features indicating the hydrothermal fluid generation.

ACKNOWLEDGMENTS

We thank A.Fallick, V.B. Naumov, O.V. Mironova, L.P. Nosik, G.N. Muravitskaya, Nat.E. Sergeeva and S.E. Borisovsky for carrying out the analytical procedures. The manuscript was significantly improved by constructive and helpful reviews from Prof. Hugo de Boorder and an anonymous reviewer. Olga Plotinskaya is thanked for reviewing an earlier version of this manuscript. The authors also thank Alexander Yakubchuk for careful and constructive editorial review of the final version of the manuscript.

The study was supported by the Russian Scientific Foundation (project no. 14-17-00693-P).

REFERENCES

Aleshin, V.M., Biyanov, I.S., 1972. Geological map of the Urals, scale 1:50000, 0-41-98-G and 0-41-110-B. Report for 1968-1972 (in Rus.).

Ayarza, P., Brown, D., Alvarez-Marro´n, J., Juhlin, C., 2000. Contrasting tectonic history of the arc–continent suture in the Southern and Middle Urals: implications for the evolution of the orogen. J. Geol. Society. 157, 1065–1076.

Baker, T., 2002. Emplacement depth and CO_2-rich fluid inclusions in intrusion-related gold deposits. Econ. Geol. 97, 1109–1115.

Baksheev, I.A., Prokof'ev, V.Yu., Ustinov, V.I., 2001. Genesis of metasomatic rocks and mineralised veins at the Berezovskoe deposit, Central Urals: Evidence from fluid inclusion and stable isotopes. Geoch. Intern. 39, Suppl.2, 129–144.

Bea, F., Fershtater, G.B., Montero, P., Smirnov, V.N, Zin'kova, E., 1997. Generation and evolution of subduction-related batholiths from Central Urals: constraints on the P-T-history of the Uralian orogen. Tectonophys. 276 (1), 103–116.

Bea, F., Fershtater, G., Montero, P., 2002. Granitoids of the Urals: implications for the evolution of the orogen. In: Brown, D., Juhlin, C., Puchkov, V. (Eds.), Mountain Building in the Uralides: Pangea to Present. Geophysical Monograph, 132. Am. Geoph. Uni. 211–232.

Bellavin, O.V., Vanshal, O.V., Nirenshtein, V.A., 1970. Shartash granite pluton, Middle Urals and related gold mineralisation. Izv. AN SSSR. Ser. Geol. 6, 86–90 (in Rus.).

Bodnar, R.J., Vityk, M.O., 1994. Interpretation of microthermometric data for H_2O–NaCl fluid inclusions. In: De Vivo, B., Frezzotti, M.L. (Eds), Fluid Inclusions in Minerals: Methods and Applications. Siena, Pontignano, 117–130.

Bohlke, J.K., 1982. Orogenic (metamorphic-hosted) gold–quartz veins. U.S. Geol. Surv., Open-file Rep. 795, 70–76.

Borisenko, A.S., 1977. Cryometric analysis of salt composition from fluid inclusions in minerals. Geol. Geophys. 18, 16–27.

Borodaevskii, N.I., Borodaevskaya, M.B., 1947. The Berezovsk Ore Field. Metallurgizdat, Moscow (in Rus.).

Borodaevskaya, M.B., Rozhkov, I.S., 1974. The ore deposits of USSR. V.3. Nedra, Moscow. 5–77 (in Rus.).

Bortnikov, N.S., Vikent'eva, O.V., Fallick, A., Sazonov, V.N., 2001. REE and Y distribution and O and D isotope study of minerals from listvenites at the Berezovsk giant mesothermal gold lode deposit, Urals, Russia: Evidence for contribution of magmatic fluid. Mineral Deposits at the Beginning of the 21st Century. Balkema, Rotterdam, pp. 707–710.

Bortnikov, N.S., Sazonov, V.N., Vikent'eva, O.V., Vikent'ev, I.V., Murzin, V.V., Naumov, V.B., Nosik, L.P., 1998. Role of the magmatogenic fluid in the formation of the mesothermal Berezovsk gold-quartz deposit, the Urals. Dokl. Earth Sci. 363 (8), 1078–1081.

Bortnikov, N.S., Vikentyev, I.V., 2013. Endogenous metallogeny of the Urals. Proc. 12th Bien. SGA Meet. Uppsala, Sweden. 1508–1511.

Bortnikov, N.S., Vikentyev, I.V., Safonov, Y.G., Zvyagina, O.V., Sazonov, V.N., Murzin V.V., Naumov, V.B., Mironova, O.V., 1997. The Berezovsk giant gold quartz deposit, Urals, Russia, in Papunen, H., ed., Minerals Deposits. Research and Exploration – Where Do They Meet? Balkema, Rotterdam, pp.157–160.

Bowers, T.S., 1991. The deposition of gold and other metals. Pressure-induced fluid immiscibility and associated stable isotope signatures. Geochim. Cosmochim. Acta. 55, 2417–2434.

Bowers, T.S., Helgeson, H.C., 1983. Calculation of the thermodynamic and geochemical consequences of nonideal mixing in the system H_2O-CO_2-NaCl on phase relations in geologic systems: Equation of state for H_2O-CO_2-NaCl fluids at high pressures and temperatures. Geochim. Cosmochim. Acta. 47, 1247–1276.

Boyle, R.W., 1979. The geochemistry of gold and its deposits. Bull. Geol. Surv. Can. 280.

Brown, P., 1989. FLINCOR: a computer program for the reduction and investigation of fluid inclusion data. Am. Mineral. 74, 1390–1393.

Brown, D., Juhlin, C., Tryggvason, A., Steer, D., Ayarza, P., Beckholmen, M., Rybalka, A., Bliznetsov, M., 2002. The crustal architecture of the Southern and Middle Urals from the URSEIS, ESRU, and Alapaev reflection seismic surveys. In: Brown, D., Juhlin, C., Puchkov, V. (Eds.), Mountain Building in the Uralides: Pangea to Present. Geophysical Monograph. 132. Am. Geoph. Union. pp. 33–48.

Brown, D., Juhlin, C., Tryggvason, A., Friberg, M., Rybalka, A., Puchkov, V., Petrov, G., 2006. Structural architecture of the Southern and Middle Urals foreland from reflection seismic profiles. Tectonics. 25, 1–12. doi:10.1029/2005TC001834.

Brown D., Juhlin C., Ayala C., Tryggvason A., Bea F., Alvarez-Marron J., Carbonell R., Seward D., Glasmacher U., Puchkov V., Perez-Estaun A., 2008. Mountain building processes during continent–continent collision in the Uralides. Earth Sci. Rev. 89, 177–195.

Burrows, D.R., Wood, P.C., Spooner, E.T.C., 1986. Carbon isotope evidence for a magmatic origin for Archean gold-quartz vein ore deposits. Nature. 321, 851–854.

Bychkov, A.Yu., 2012. The transfer and concentration of elements in heterogeneous hydrothermal systems. Dr. Sci. Thesis. Lomonosov Moscow State University, Moscow.

Chesnokov, B.V., 1973. Endogenous zoning of the Berezovsk ore field in the middle Urals. Dokl. Earth Sci. 210 (4), 915–917 (in Rus.).

Cox, S., 2016. Injection-driven swarm seismicity and permeability enhancement: Implications for the dynamics of hydrothermal ore systems in high fluid-flux, overpressured faulting regimes. Econ. Geol., Bull. Soc. Econ. Geol. 111 (3), 559-587.

Crawford, M.L., 1981. Phase equilibria in aqueous fluid inclusions. Fluid Inclusions: Applications to Petrology: Mineral. Ass. Canada. Short Course. Handbook. 6, 75–100.

Davis, D.W., Lowenstein, T.K., Spenser, R.J., 1990. Melting behavior of fluid inclusions in laboratory-grown halite crystals in the systems NaCl-H_2O, NaCl-KCl-H_2O, NaCl-$MgCl_2$-H_2O and $CaCl_2$-NaCl-H_2O. Geochim. Cosmochim. Acta. 54, 591–601.

De Boorder, H., 2012. Spatial and temporal distribution of the orogenic gold deposits in the Late Palaeozoic Variscides and Southern Tianshan: How orogenic are they? Ore Geol. Rev. 46, 1–31.

Emmons, W.H., 1937. Gold deposits of the World. McGraw-Hill Book Company, New York-London.

Fershtater, G.B., 2013. Palaeozoic intrusive magmatism of the Middle and South Urals. Ural Branch of RAS, Ekaterinburg (in Rus.).

Fershtater, G.B., Kholodnov, V.V., Kremenetskii, A.A., Krasnobaev, A.A., Borodina, N.S., Zin'kova, E.A., Pribavkin, S.V., 2010. Au-bearing gabbro-tonalite-granodiorite-granite plutons of the Urals: age, geochemistry, and magmatic and ore evolution. Geol. Ore Dep. 52(1), 58–76.

Faure, G., 1986. Principles of isotope geology, second ed. John Wiley and Sons, New York.

Garofalo, P.S., Fricker, M.B., Güntner, D., Bersani, D., Lottici, P.P., 2014. Physical-chemical properties and metal budget of Au-transporting hydrothermal fluids in orogenic deposits. In: Garofalo, P.S., Ridley, J.R. (Eds) Gold-Transporting Hydrothermal Fluids in the Earth's Crust. Geol. Society, London. pp. 71–102.

Goldfarb, R.J., Groves, D.I., 2015. Orogenic gold: Common or evolving fluid and metal sources through time. Lithos. 233, 2–26.

Goldfarb, R.J., Phillips, G.N., Nockleberg, W.J., 1998. Tectonic setting of synorogenic gold deposits of the Pacific Rim. Ore Geol. Rev. 13, 185–218.

Goldfarb, R.J., Baker, T., Dubé, B., Groves, D.I., Hart, C.J.R., Robert, F., Gosselin, P., 2005. World distribution, productivity, character, and genesis of gold deposits in metamorphic

terranes. In Hedenquist, J.W., Thompson, J.F.H., Goldfarb, R.J., Richards, J.P. (Eds.). Econ. Geol. One Hundredth Anniversary Volume 1905–2005, Soc. of Econ. Geol. 407–450.

Goryachev, N.A., Pirajno, F., 2014. Gold deposits and gold metallogeny of Far East Russia. Ore Geol. Rev. 59, 123–151.

Groves, D.I., Goldfarb, R.J., Gebre-Mariam, M., Hagemann, S.G., Robert, F., 1998. Orogenic gold deposits: a proposed classification in the context of their crustal distribution and relationships to other gold deposit types. Ore Geol. Rev. 13, 7–27.

Groves, D.I., Goldfarb, R.J., Robert, F., Hart, C.J.R., 2003. Gold deposits in metamorphic belts: Overview of current understanding, outstanding problems, future research, and exploration significance. Econ. Geol. 98, 1–29.

Gzovskii, M.V., 1975. Basics of Tectonophisics. Nauka, Moscow (in Rus.).

Hackbarth, C.J., Petersen, U.A., 1984. Fractional crystallisation model for the deposition of argentian tetrahedrite. Econ. Geol. 79, 448–460.

Hart, C.J.R., 2005. Classifying, distinguishing and exploring for intrusion-related gold systems. The Gangue, Geological Association of Canada, Mineral Deposits Division Newsletter, 87(1), 4–9.

Hart, C.J.R., 2007. Reduced intrusion-related gold systems. In: Goodfellow, W.D. (Ed.), Mineral deposits of Canada: A Synthesis of Major Deposit Types, District Metallogeny, the Evolution of Geological Provinces, and Exploration Methods. Geological Association of Canada, Mineral Deposits Division, Special Publication No. 5, pp. 95–112.

Hart, C.J.R., Goldfarb, R.J., 2005. Distinguishing intrusion-related from orogenic gold system. In: New Zeland Minerals Conference Proceedings, 125–133.

Hart, C.J.R., McCoy, D., Goldfarb, R.J., Smith, M., Roberts, P., Hulstein, R., Blake, A.A., Bundtzen T.K., 2002. Geology, exploration and discovery in the Tintina gold province, Alaska and Yukon. Soc. Econ. Geol. Spec. Publ. 9, 241–274.

Hedenquist, J.W., Lowenstern, J.B., 1994. The role of magmas in the formation of hydrothermal ore deposits. Nature. 370, 519–527.

Herrington, R.J., Puchkov, V.N., Yakubchuk, A.S., 2005. A reassessment of the tectonic zonation of the Uralides: implications for metallogeny. Geol. Soc. London Spec. Publ. 248(1), 153–166 DOI:10.1144/GSL.SP.2005.248.01.08

Hoefs, J., 1987. Stable Isotope Geochemistry. Springer, Berlin.

Igumnov, S.A., Perkova, R.I., Chesnokov, B.V., 1977. Zonal distribution of sulphur isotopes in pyrite crystals and some formation features of the sulphide mineralisation of the Berezovsk gold deposit in the Urals. Geochem. Intern. 9, 1407–1412.

Ivanov, S.N, Perfiliev, A.S, Efimov, A.A, Smirnov, G.A, Necheukhin,V.M, Fershtater, G.B, 1975. Fundamental features in the structure and evolution of the Urals. Am. J. Sci. 254, 107–136.

Jia, Y., Li, X, Kerrich, R., 2001. Stable isotope (O, H, S, C, and N) systematic of quartz vein systems in the turbidite-hosted Central and North Deborah gold deposits of the Bendigo Gold Field, Central Victoria, Australia: Constraints on the origin of ore-forming fluids. Econ. Geol. 96, 705–721.

Kalyuzhny, V.A., 1982. Principles of the theory on mineral-forming fluids. Naukova Dumka, Kiev. (in Rus.)

Kerrich, R., Fryer, B.J., 1988. Lithophile-element systematics of Archean greenstone belt Au-Ag vein deposits: implications for source processes. Can. J. Earth Sci. 25, 945–953.

Kerrich, R., Fyfe, W.S., 1981. The gold carbonate association: source of CO_2 fixation reactions in Archean lode deposits. Chem. Geol. 33, 265–294.

Kerrich, R., Goldfarb, R.J., and Richards, J., 2005, Metallogenic provinces in an evolving geodynamic framework. Econ. Geol. 100th Anniv. Vol., 1097–1136.

Kleymenov, D.A., Albrecht, V.G., Erokhin, Yu.V., Batalin, A.S., Batalina, A.A, 2005. Berezovsk gold deposit: the history and mineralogy. Ural. Worker, Yekaterinburg (in Rus.).

Knopf, A., 1929. The Mother Lode system of California. U. S. Geol. Surv. Prof. Paper. 157, 103.

Konovalova, E.V., Pribavkin, S.V., Zamyatin, D.A., Kholodnov, V.V., 2012. Sulphur in apatite from Shartash granite massif and Berezovsk gold deposit. Yearbook-2011, Inst. Geol. Geochim. Uralian Branch RAS, Yekaterinburg, 134–138 (In Rus.).

Konstantinov, M.M., Kosovets, T.N., Kryazhev, S.G., Natalenko, M.V., Struzhkov, S.F., Ustinov, V.I., 2002. The structure and development of gold-bearing ore-forming systems. TsNIGRI, Moscow (in Rus.).

Kontak, D.J., Kyser, K., 2011. A fluid inclusion and isotopic study of an intrusion-related gold deposit (IRGD) setting in the 380 Ma South Mountain Batholith, Nova Scotia, Canada: evidence for multiple fluid reservoirs. Mineral. Dep. 46, 337–363.

Koroteev, V.A., De Boorder, H., Necheukhin, V.M., Sazonov, V.N., 1997. Geodynamic setting of the mineral deposits of the Urals. Tectonophys. 276, 291–300.

Khramov, D.G., 2014. The status and use of mineral resources of the Russian Federation in 2013. State report (in Rus.).

Kryazhev, S.G., Grinenko, V.A., Ustinov, V.I., 2011. Possible reasons for the compositional evolution of ore-forming fluids at the Berezovsk gold deposit, Central Urals. Geochem. Intern. 49(1), 95–100.

Kutyukhin, P.I., 1948. The conditions for the localisation of mineralisation in the veins of Berezovsk deposit, in: Ivanov, A.A., Rozhkov, I.S. (Eds.) 200 years of the gold industry of the Urals. Uralian Branch Acad. Sci. USSR, Sverdlovsk. pp. 249–275 (In Rus.).

Kutyukhin, P.I., Borodaevskii, N.I., Borodaevskaya M.B., 1947. About the composition of ores and near-vein alteration at the Berezovsk vein field. Soviet Geol. 14–15, 110–116 (In Rus.).

Kyzer, T.K., 1987. Stable isotope geochemistry of low temperature fluids. Mineral. Ass. Can. Short Course. 13, 287–336.

Lang, J.R., Baker, T., Hart, C.J.R., Mortensen, J.K., 2000. An exploration model for intrusion-related gold systems. Soc. Econ. Geol., Newsletter. 40, 1–15.

Li, Y.B., Liu, J.M., 2006. Calculation of sulphur isotope fractionation in sulphides. Geochim. Cosmochim. Acta. 70, 1789–1795.

Lindgren, W., 1933. Mineral deposits, fourth ed. McGraw - Hill Book Company, New York-London.

Matsuhisa, Y., Goldsmith, J.R., Clayton, R.N., 1979. Oxygen isotopic fractionation in the system quartz–albite–anorthite–water. Geochim. Cosmochim. Acta. 43,1131–1140.

McCoy, D., Newberry, R.J., Layer, P., DiMarchi, J.J., Bakke,A., Masterman, S., Minehane, D.L., 1997. Plutonic-related gold deposits of Interior Alaska, in Goldfarb, R.J., Miller, L.D. (Eds.), Mineral Deposits of Alaska. Econ. Geol. Monogr. 9, 191–241.

McKay, B., Wake, B., 2006. Intrusion-related gold system in the New England fold belt – the Tooloom example. Malachite Resources. 95–103.

McKibben, M.A., Eldridge, C.A.S., 1990. Radical sulphur isotope zonation of pyrite accompanying boiling and epithermal gold deposition: a SHRIMP study of the Valles Caldera, New Mexico. Econ. Geol. 85, 1917–1925.

Murzin. V.V., Talantsev, A.S., Leont'ev, R.L., 1987. Native gold on the deep level of the Berezovsk deposit (Urals). Izv. AN SSSR. Ser. Geol. 5, 70–79 (in Rus.).

Nesbitt, B.E., Murowchick, J.B., Muehlenbachs, K., 1986. Dual origins of lode gold deposits in the Can. Cordillera. Geol. 14, 506–509.

Newberry, R.J., McCoy, D.T., Brew, D.A., 1995. Plutonic-hosted gold ores in Alaska: Igneous vs. metmorphic origins. In: Ishihara S., Czamanske G.K. (Eds.). Proc. Sapporo International Conf. on Mineral Resources of the NW Pacific Rim. Res Geol, Spec Iss. 18, 57–100.

Ojala, V.J., Groves, D.I., Ridley, J.R., 1995. Hydrogen isotope fractionation factors between hydrous minerals and ore fluids at low temperatures: evidence from the Granny Smith gold deposit, Western Australia. Mineral. Dep. 30, 328–331.

O'Neil, J.R., Taylor, H.P.Jr., 1969. Oxygen isotope fraction between muscovite and water. J. Geophys. Res. 74, 6012–6022.

Ohmoto, H., 1986. Stable isotope geochemistry of ore deposits. Rev. Mineralogy. 16, 491-560.

Ohmoto, H., 1972. Systematic of sulphur and carbon isotopes in hydrothermal ore deposits. Econ.Geol. 67, 551–578.

Ohmoto, H., Rye, R.O., 1979. Isotopes of sulphur and carbon, in Barnes, H.L. (Ed.), Geochemistry of Hydrothermal Ore Deposits. J.Willy., Sons, New York, pp. 509–567.

Ovchinnikov, L.N., 1998. Mineral Resources and Metallogeny of the Urals. Geoinformmark, Moscow (in Rus.).

Petrovskaya, N.V., 1972. Native Gold. Nauka, Moscow (in Rus.).

Pirajno, F., 2009. Hydrothermal Processes and Mineral Systems. Springer, Berlin.

Phillips, G.N., Powell, R., 1993. Link between gold provinces. Econ. Geol. 88, 1084–1098.

Phillips, G.N., Powell, R., 2010. Formation of gold deposits – a metamorphic devolatilisation model. J. Metamorphic Geol. 28, 689–718.

Poulson, S.R., Kubilius, W.P., Ohmoto, H., 1991. Geochemical behaviour of sulphur in granitoids during intrusion of the South Mountain Batholith, Nova Scotia, Canada. Geochim. Cosmochim. Acta. 55, 3809–3830.

Puchkov, V.N., 1997. Tectonics of the Urals – modern concepts. Geotectonics. 31, 294–312.

Puchkov, V.N., 2000. Palaeogeodynamics of the Southern and Middle Urals. Dauriya, Ufa (in Rus.).

Puchkov, V.N., 2017. General features relating to the occurrence of mineral deposits in the Urals: What, where, when and why. Ore Geol. Rev. 85, 4–29.

Pribavkin, S.V., Pushkarev, E.V., 2011. The age of late orogenic granitoids of the Urals based on U-Pb isotope dating of zircons (exemplified by the Shartash and Shabry massifs). Dok. Earth Sci. 438(1), 627–631.

Pribavkin, S.V., Ronkin, Yu.L., Travin, A.V., Ponomarchuk, V.A., 2007. New data on the age of lamproite-lamprophyre magmatism in the Urals. Dok. Earth Sci. 413(2), 213–215.

Rapoport, M.S., Babenko, V.V., Boltyrev, V.B., 1994. Berezovsk gold deposit. Izv.Vyssh. Uchebn. Zaved. Gorny Zhurnal. 6, 86–96 (in Rus.).

Ridley, J.R., Diamond, L.W., 2000. Fluid chemistry of orogenic lode-gold deposits and implications for genetic models. Rev. Econ. Geol. 13, 141–162.

Roedder, E., 1984. Fluid inclusions. Min. Soc. Am. Rev.Mineral. 12.

Rose, G., 1837. Mineralogisch-geognostische Reise nach dem Ural, dem Altai und dem Kaspischen Meere. Vol.1. Reise nach demnördlichen Ural und dem Altai. Sandersche Buchhandlung, Berlin.

Samartsev, I.T., Zakhvatkin, V.A., Kazimirskii, V.F., 1973. On the zonation of the Berezovsk gold deposit in the Middle Urals. Geol. Ore Dep. 1, 110–117 (in Rus.).

Samartsev, I.T., Egorova, N.A., Guseva, L.D., 1985. Study of structure and location of gold ores on deep level of the Berezovsk deposit and Stanovlyan field. Report. Tula (in Rus.).

Sack, R.O., Brackebusch, F.W., 2004. Fahlore as an indicator of mineralisation temperature and gold fineness. Can. Mining Metall. Bull. 97(1081), 78–83.

Sack, R.O., Loucks R.R., 1985. Thermodynamic properties of tetrahedrite-tennantites: constraints on the interdependence of the Ag↔Cu, Fe↔Zn, Cu↔Fe, and As↔Sb exchange reactions. Am. Mineral. 70, 1270–1289.

Sazonov, V.N., Grigoriev, N.A., Murzin, V.V., 1993. The gold of the Urals. Inst. Geol. Geochim., Uralian Branch, RAS, Ekaterinburg. (in Rus.).

Sazonov, V.N., Ogorodnikov, V.N., Koroteev, V.A., Polenov, Yu., 1999. Gold deposits of the Urals. UGGGA, Ekaterinburg (in Rus.).

Sazonov, V.N., 1984. The beresite-listvenite formation. Ural. Branch Akad. Sci. USSR, Sverdlovsk. (in Rus.).

Sazonov, V.N. 1975. Listvenitisation and ore mineralisation. Nauka, Moscow. (in Rus.).

Sazonov, V.N., van Herk, A.H., de Boorder, H., 2001. Spatial and temporal distribution of gold deposits in the Urals. Econ. Geol. 96, 685–703.

Shaw, D*.M.*, 1968. A review of K-Rb fractionation trends by covariance analysis. Geochim. Cosmochim. Acta. 32, 573–601.

Shelton, K.L., So, C.S., Chang, J.S., 1988. Gold-rich mesothermal vein deposits of the Republic of Korea: Geochemical studies of the Jungwon gold area. Econ. Geol. 83(6), 1221–1237.

Sheppard, S.M.F., 1986. Characterisation and isotopic variations in natural water. Rev. Mineral. 16, 165–183.

Sherlock, R.L., Roth, T., Spooner, E.T.C., Bray, C.J., 1999. Origin of the Eskay Creek precious metal-rich volcanogenic massive sulfide deposit: fluid inclusion and stable isotope evidence. Econ. Geol. 94, 803–824.

Sibson, R.H., Robert, F., Poulson, K.H., 1988. High-angle reverse faults, fluid pressure cycling and mesothermal gold-quartz deposits. Geology. 16, 551–555.

Sillitoe, R.H., 1991. Intrusion-related gold deposits, in: Foster, P.R., (Ed.), Gold Metallogeny and Exploration. Blackie and Son, Glasgow, pp. 165–209.

Sillitoe, R.H., Thompson, J.F.H., 1998. Intrusion-related vein gold deposits: types, tectono-magmatic settings and difficulties of distinction from orogenic gold deposits. Resource Geology. 48(2), 237–250.

Smirnov, V.I., 1982. Geology of mineral resource. Nedra, Moscow (in Rus.).

Sobolev, I.D., 1983. Tectonic map of the Urals, scale 1:1000000. Nedra, Sverdlovsk.

Spenser, R.J., Moller, N., Weare, J.H., 1990. The prediction of mineral solubilities in mineral waters: a chemical equilibrium model for the Na-K-Ca-Mg-Cl-SO_4 system at temperatures below 25°C. Geochim. Cosmochim. Acta. 54, 575–602.

Spiridonov, E.M., Baksheev, I.A., Seredkin, M.V., Prokof'ev, V.Yu., Ustinov, V.I., Filimonov, S.V., 1998. Gumbeites and associated ore mineralisation of the Urals (Russia). Geol. Ore Dep. 40, 152–171.

Thompson, J.F.H., Newberry, R.J., 2000. Gold deposits related to reduced granitic intrusions. Rev. Econ. Geol. 13, 377–400.

Thompson, J.F.H., Sillitoe, R.H., Baker, T., Lang, J.R., Mortensen, J.K., 1999. Intrusion-related gold deposits associated with tungsten-tin provinces. Mineral. Dep. 34, 323–334.

Tomkins, A.G., 2013. On the source of orogenic gold. Geology. 41(12), 1255–1256.

Vikent'eva, O.V., 2000a. Berezovsk gold deposit in the Urals: geological structure, mineralogical and geochemical features and formation conditions. Ph D Thesis. Lomonosov Moscow State University, Moscow (in Rus.).

Vikent'eva, O.V., 2000b. Mineral and metal zoning at the Berezovsk gold deposit. Metallogeny of ancient and modern oceans – 2000. Inst. Mineral., Uralian Branch, RAS, Miass. pp. 208-214 (in Rus.).

Vikent'eva, O.V., Bortnikov, N.S., Murzin, V.V., Naumov, V.B., 2000. Fluid regime of mineral formation at the Berezovsk gold deposit. Yearbook-1999, Inst. Geol. Geochim., Uralian Branch, RAS, Yekaterinburg, 224–227 (in Rus.).

Wenner, D.B. Taylor, H.P. Jr., 1971. Temperatures of serpentinisation of ultramafic rocks based on O^{16}/O^{18} fractionation between coexisting serpentine and magnetite. Contrib. Mineral. Petrol. 32, 165–185.

Wesolowskii, D., Ohmoto, H., 1986. Calculated oxygen isotope fractionation between water and the minerals scheelite-powellite. Econ. Geol. 81, 471–477.

Wilkinson, J.J., 1990. The role of metamorphic fluids in the development of the Cornubian orefield: fluid inclusion evidence from south Cornwall. Mineral. Magazine. 54(375), 219–230.

White, W.M., 2015. Isotope Geochemistry, Wiley-Blackwell.

Yakubchuk, A., 2017. Evolution of the Central Asian Orogenic Supercollage since Late Neoproterozoic revised again. Gondwana Research. 47, 372-398.

Yakubchuk, A., Cole, A., Seltmann, R., Shatov, V.V., 2002. Tectonic setting, characteristics, and regional exploration criteria for gold mineralisation in the Altaid tectonic collage: the Tien Shan province as a key example. Soc.Econ. Geol., Spec. Publ. 9, 177–201.

Yardley, B.D., Bodnar, R.J., 2014. Fluids in the Continental Crust. Geochemical perspectives. 3 (1).

Yardley, B.W.D., Cleverley, J.S., 2013. The role of metamorphic fluids in the formation of ore deposits. Geol. Soc. London Spec. Publ. 393, 117-134. doi: 10.1144/SP393.5.

Yardley, B., Gleeson, S., Bruce, S., Banks, D., 2000. Origin of retrograde fluids in metamorphic rocks. J. Geoch. Explor. 69-70, 281-285.

Yazeva, R.G., Bochkarev, V.V., 1996. Silurian island arc of the Urals: structure, evolution and geodynamics. Geotectonics. 29, 478–489.

Zaraisky, G.P., 1989. Zoning and formation conditions of metasomatic rocks. Nauka, Moscow.

Zbou, T., Dobos, S.K., 1995. A carbon and oxygen stable isotopic study of the siderite alteration in the Black Ridge gold deposit, Clermont, Central Queesland. Mineral. Dep. 30(1), 30–38.

Fig. 1. Tectonic map (**a**; modified after Puchkov, 2010) and regional geological map (**b**; modified after Sobolev, 1983) showing the Berezovsk deposit setting.

Fig. 2. Geological map (**a**) and cross-section (**b**) of the Berezovsk deposit (modified after Rapoport et al., 1994). Coordinate grid through 1 km corresponds to Berezovsk mine coordinate system.

Fig. 3. Morphology of the auriferous sulphide-quartz veins: **a** – Relationships between ladder and “krassyk” veins. The Andreevskaya dyke of granite-porphyry and Molokovskie krassyk veins, level 62 m; **b** – Ladder veins in Krivaya dyke. Kirov mine, level 112 m (after N.Levkovich).

Fig. 4. The auriferous "ladder" veins: **a** – carbonate-quartz *en echelon* veinlets and sulphide vein; **b** – quartz vein with minor sulphides; **c** – pyrite-quartz vein with halo of beresitisation; **d** – sulphide-quartz vein (predominant galena). a, b, c – Vtoropavlovskaya dyke, level 444 m; d – Soedinennaya dyke, level 314 m.

Fig. 5. Complicated morphology of the ladder veins filling shear fractures (two systems) and ruptures. Elizavetinskaya dyke, level 262 m. **a** – block 120, the western wall of the southern drift; **b** – block 120, the eastern wall of the southern drift; **c** – block 120, block 120, the eastern wall of the northern drift; **d** – block 121, the eastern wall of the northern drift; **e** – block 123, the eastern wall of the northern drift (according to the Berezovsk mine data).

Fig. 6. Morphology of the “krassyk” vein in talc-carbonate rocks. Berezovsk ore field, Lenin mine, drift roof, Molokovskie Veins (after P.I. Kutyukhin). Q – quartz, Py – pyrite.

Fig. 7. **a** – Metasomatic zoning at the contact of sulphide-quartz vein with granitoid dyke and talc-carbonate rock. Shaft 1, level 218 m (after V.N. Sazonov). Photos of beresite (**b**) and listvenite (**c**).

Fig. 8. Mineral formation sequence for the ore veins at the Berezovsk deposit. Fluid inclusion, sphalerite-tennantite (Sp-Tnt) and native gold-tennantite (Au-Tnt) geothermometry data from this study, calcite-dolomite (Cc-Dol) geothermometry (after A.S. Talantzev).

Fig. 9. Photomicrographs showing the mineral relationship for the pyrite-quartz and gold-polymetallic stages (polished sections, reflected light): **a** – Tennantite with chalcopyrite II fills the cracks in pyrite II and is brecciated on the contact with pyrite II. **b** – Fractured pyrite II in tennantite-galena-carbonate aggregate. Tennantite contains xenomorphic and veinlet-like inclusions of chalcopyrite II. **c** – Tennantite fills the fractures in pyrite II. **d** – Tennantite-calcopyrite II aggregates are crushed on the contact with pyrite II. Abbreviations: Py – pyrite, Tnt – tennantite, Gn – galena, Ccp – chalcopyrite.

Fig. 10. Photomicrographs showing the mineral assemblages in the gold-polymetalic stage (polished sections, reflected light): **a** – Chalcopyrite II-sphalerite II aggregates filling the microfissures in tennantite with relics of gersdorffite. Native gold II forms elongated crystal. **b** – Sphalerite II and chalcopyrite II overgrow the pyrite crystal in tennantite. **c-d** – Clusters of gold grains included in tennantite. Native gold II spatially associates with chalcopyrite II. **e** – Galena II occurs along the contact of sphalerite and tennantite. Sphalerite contains small blebs of chalcopyrite. Tennantite comprises veinlets of chalcopyrite and its intergrowth with native gold. Abbreviations: Py – pyrite, Tnt – tennantite, Gf – gersdorffite, Ccp – chalcopyrite, Gn – galena, Sp – sphalerite, Au – native gold.

Fig. 11. The fineness of native gold in the pyrite-quartz (Au I) and gold-polymetallic (Au II) assemblages of veins from the Berezovsk deposit. Py – pyrite, Ttd-Tnt – tetrahedrite-tennantite minerals.

Fig. 12. Chemical composition of the tennantite-tetrahedrite minerals in veins from the Berezovsk deposit. Symbols of various colours correspond to samples from different distances to the Shartash massif.

Fig. 13. Binary plots for fluid inclusions in the quartz, carbonate and sphalerite of the Berezovsk deposit. **a** – Homogenisation (T_{hom}) vs eutectic temperatures (T_{eut}), **b** - Homogenisation temperature (T_{hom}) vs salinity (C_{salt}), **c** - Salinity (C_{salt}) vs eutectic temperature (T_{eut}), **d** – Pressure (P) vs homogenisation temperature (T_{hom}).

Fig. 14. Binary plots for fluid inclusions showing the correlation with the depth of homogenisation temperature (a) and salinity (b) at the Berezovsk deposit.

Fig. 15. CO_2-H_2O-N_2 and CO_2-CH_4-N_2 ternary diagrams for fluid inclusions from vein quartz (Q) and scheelite (Sch) of the Berezovsk deposit.

Fig. 16. Summary of carbon and oxygen isotope data for vein carbonates from different dykes of the Berezovsk deposit in comparison with ranges of carbonatites and marine carbonates (after Hoefs, 1987).

Fig. 17. Sulphur isotope compositions of sulphide minerals from ore veins of the Berezovsk deposit.

Fig. 18. The δD-$\delta^{18}O$ values for fluid calculated from minerals of unaltered rocks and alteration zoning in comparison with ranges of magmatic and metamorphic water (after Sheppard, 1986). SMOW: Standart Mean Ocean Water.

Fig. 19. Mineral and metal zoning relative to the roof of the Shartash massif. **a** – isolines of the Shartash massif roof (in km); **b** – host rock alteration and ore types; **c** – productive mineral assemblages (Q-Ank – ankerite-quartz, Q-Py – pyrite-quartz, Au-sulphide – gold-polymetallic); **d** - tennantite-tetrahedrite minerals; **e** – “pulsation zoning” model by Smirnov, 1982.

Fig. 20. Schematic palaeotectonic stress fields for periods of dyke formation (**a**) and formation of sulphide-quartz "ladder" veins in the dyke (**b**) using technique of Gzovskii (1975). (**c**) – position of the sulphide-quartz veins in the dyke. σ – orientation of the principal normal axes of the compressional stress (σ_1 – maximum and σ_2 – intermediate, point line; σ_3 – minimum, dotted line); thick arrows indicate directions of maximum compression; black bold line (on Fig. **a** and **b**) is a granitoid dyke.

Fig. 21. Genetic model of the Berezovsk hydrothermal system.

Fig. 22. Schematic palaeoreconstruction of the Berezovsk deposit using geological mapping data of Borodaevskii and Borodaevskaya (1947), Aleshin and Biyanov (1972), Samartsev et al. (1985) and geophysical data by Bellavin et al. (1970). The zero level corresponds to the modern toposurface.

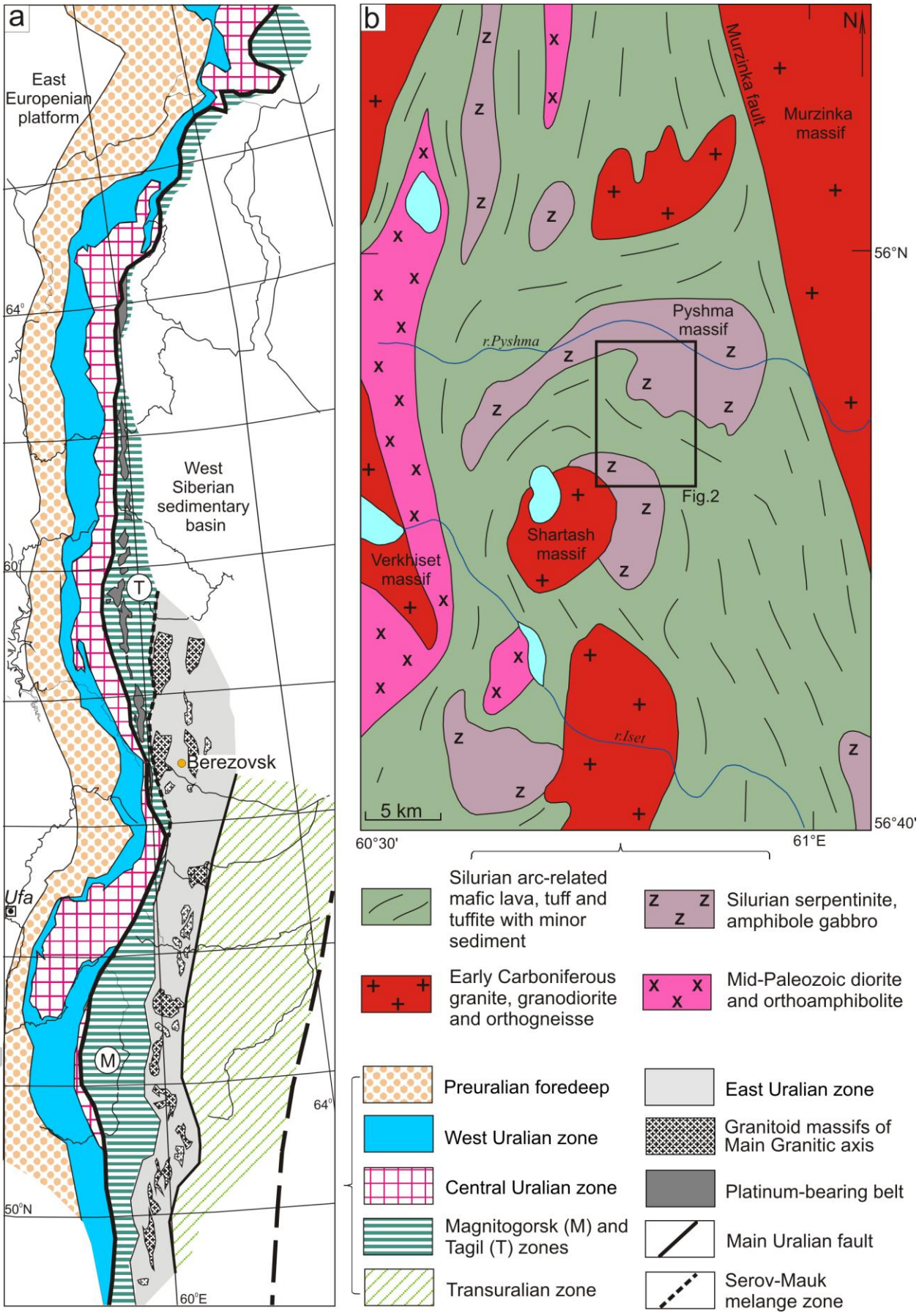

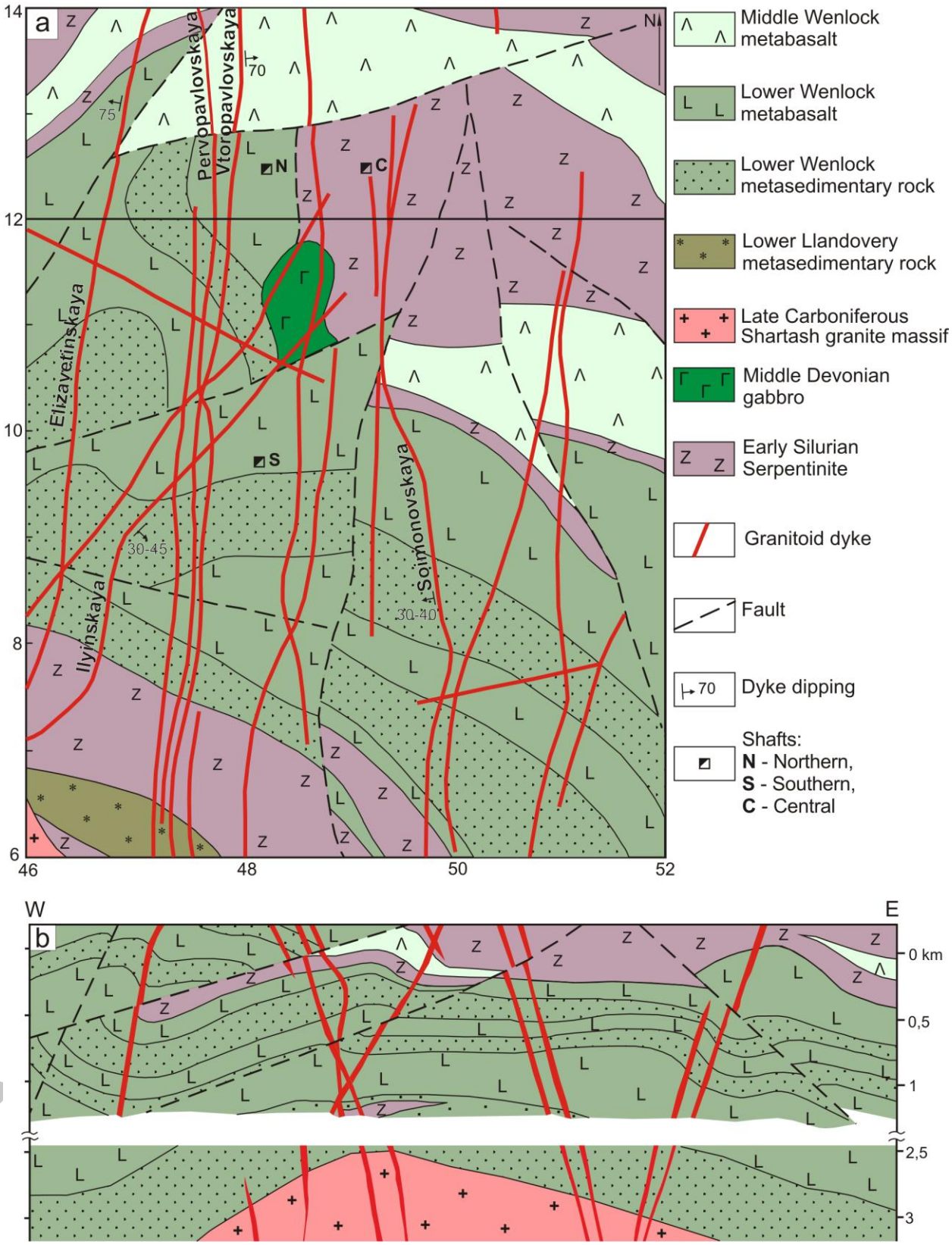

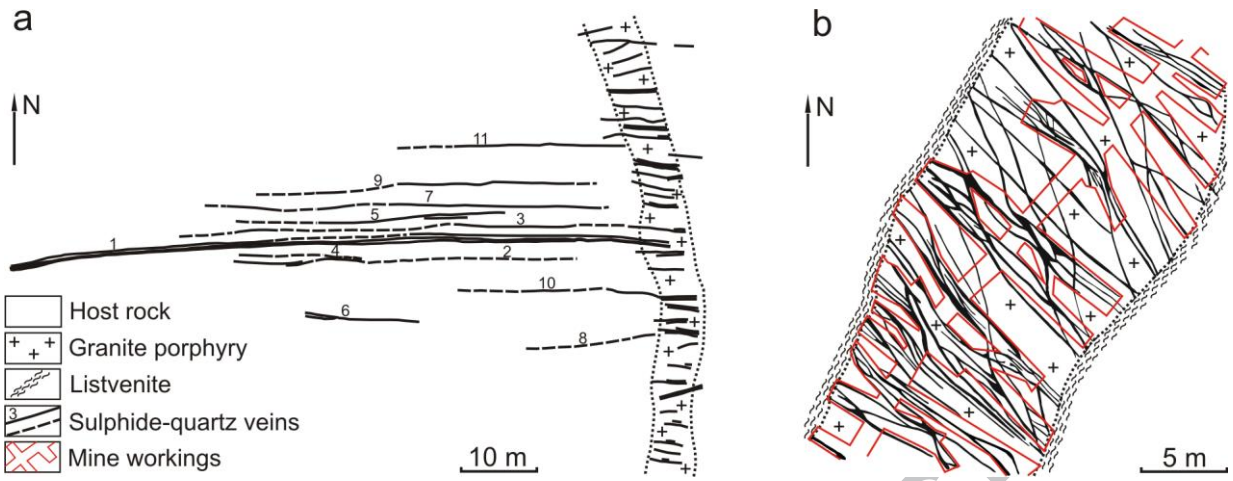

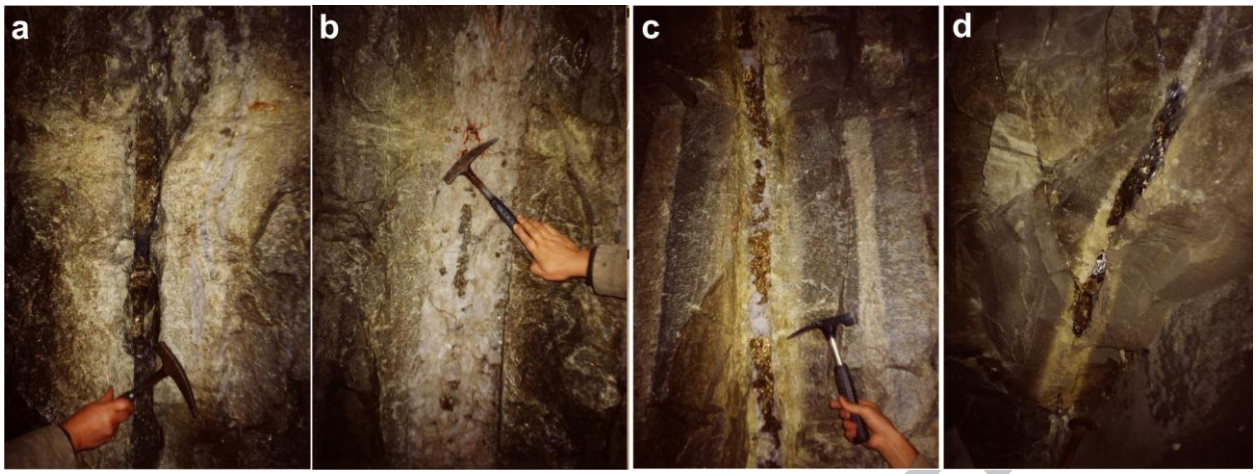

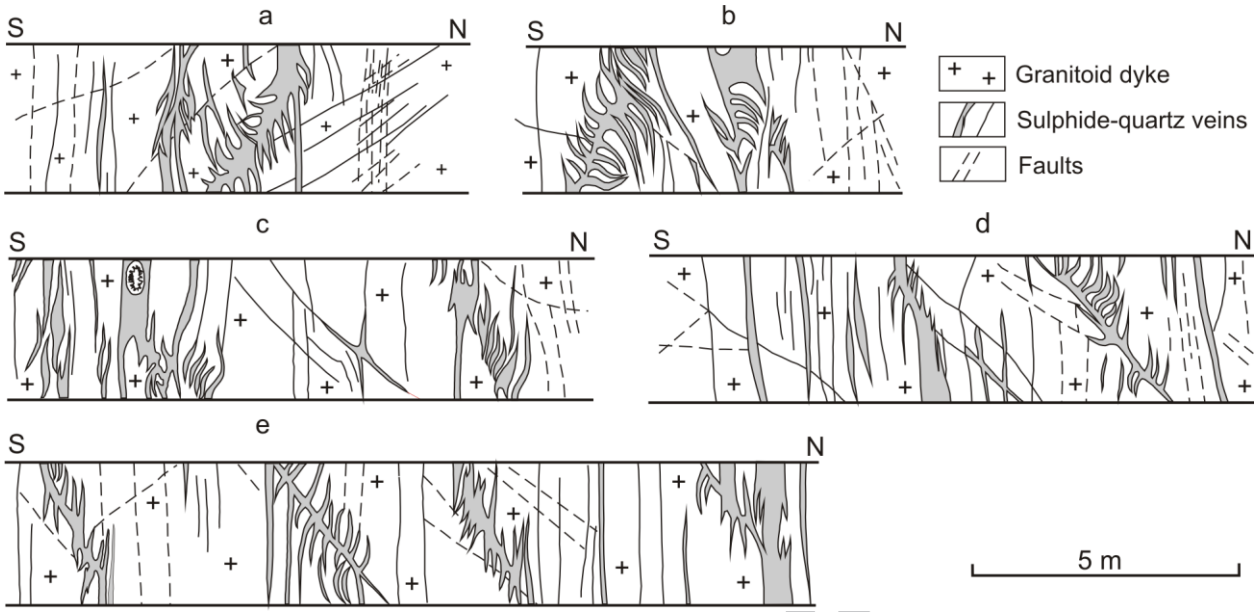

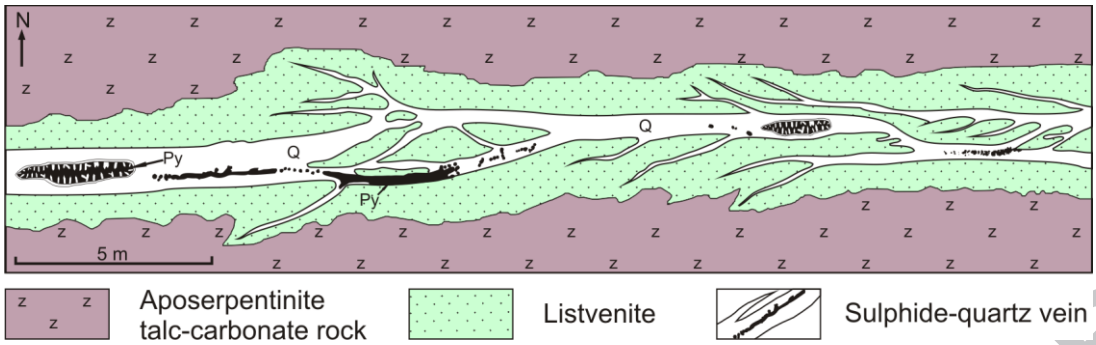

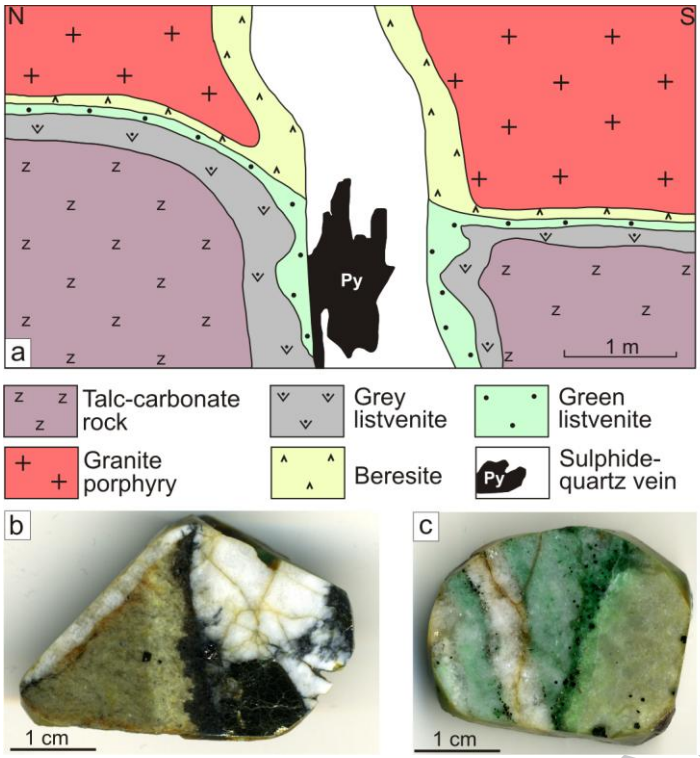

Stage / Minerals	Ankerite-quartz	Pyrite-quartz	Gold-polymetallic	Carbonate
Ankerite				
Quartz				
Pyrite	I	II	III	
Scheelite				
Tennantite				
Sphalerite		I	II	
Chalcopyrite		I	II	
Galena		I	II	
Native gold		I	II	
Aikinite				
Matildite				
Calcite				
Dolomite				
Estimated crystallization temperature, ºC				
Fluid inclusions in:				
Quartz	250-265	230-293	210-301	
Ankerite	238-250			
Sphalerite			200-233	
Mineral geothermometers:				
Sp-Tnt			150-250	
Au-Tnt			174-208	
Cc-Dol		260-360	150-260	80-160

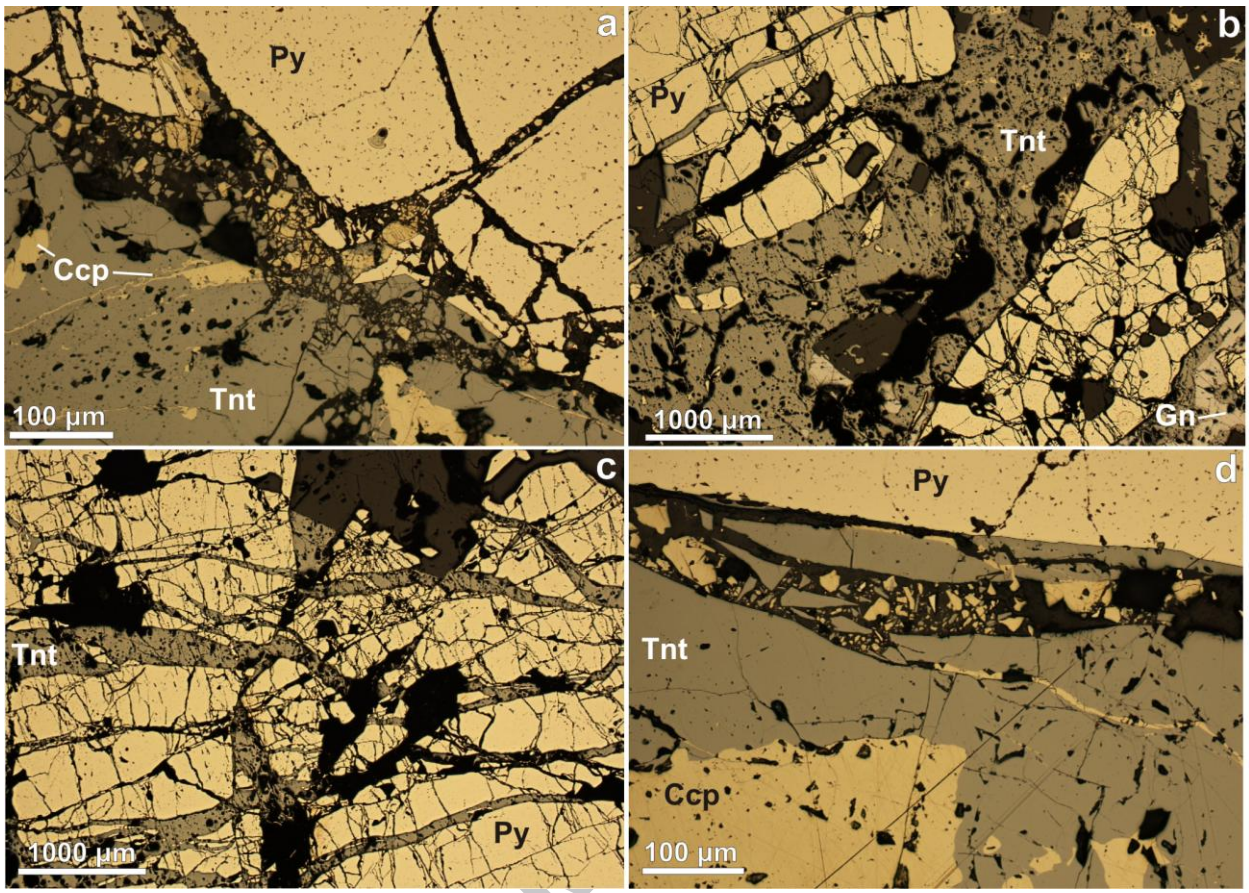

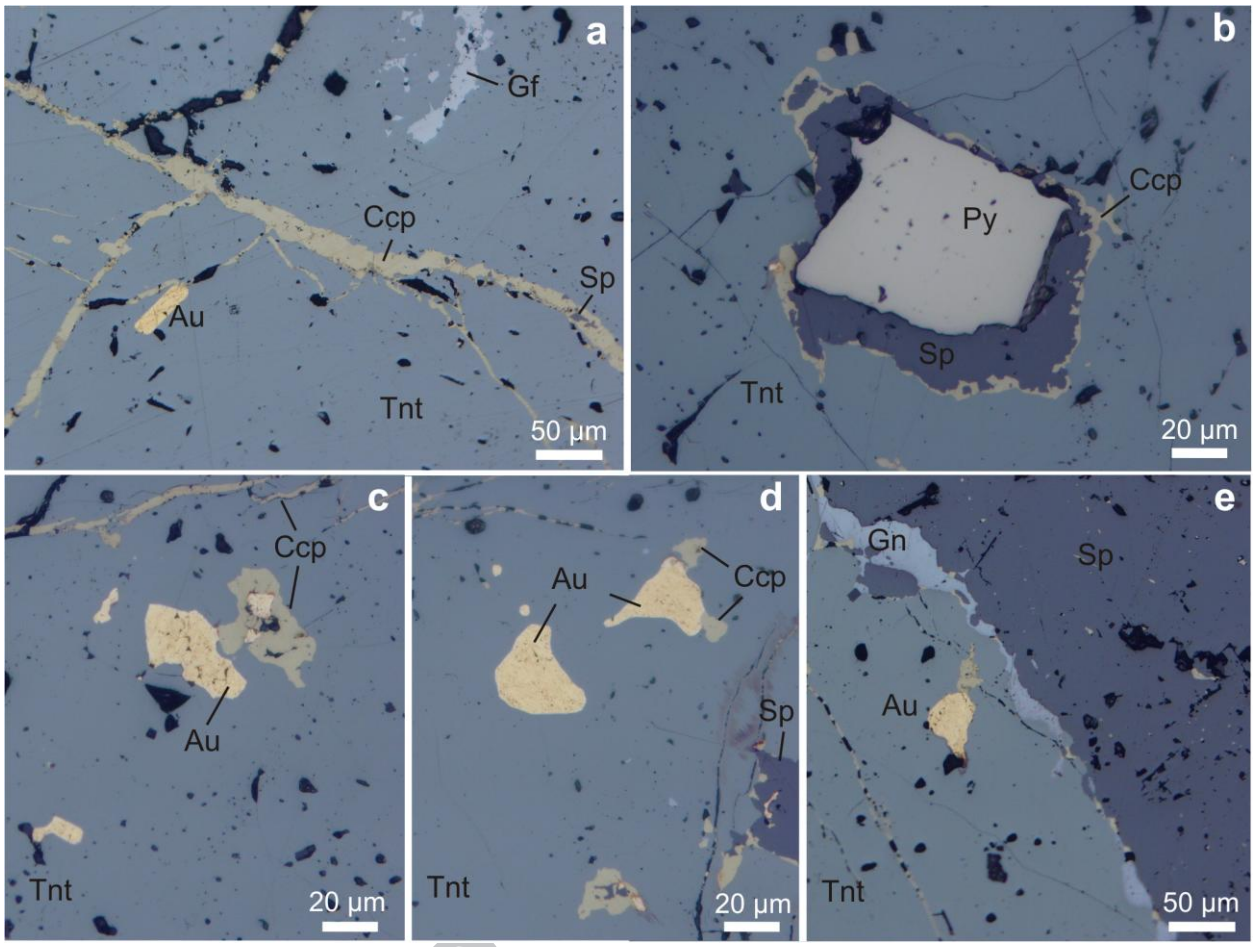

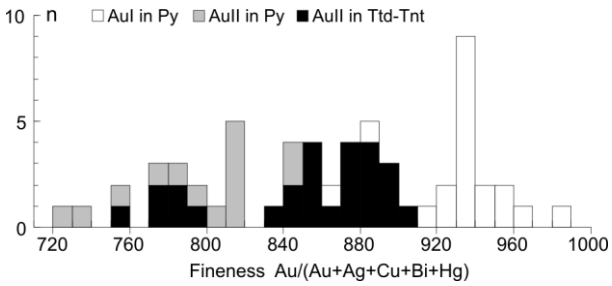

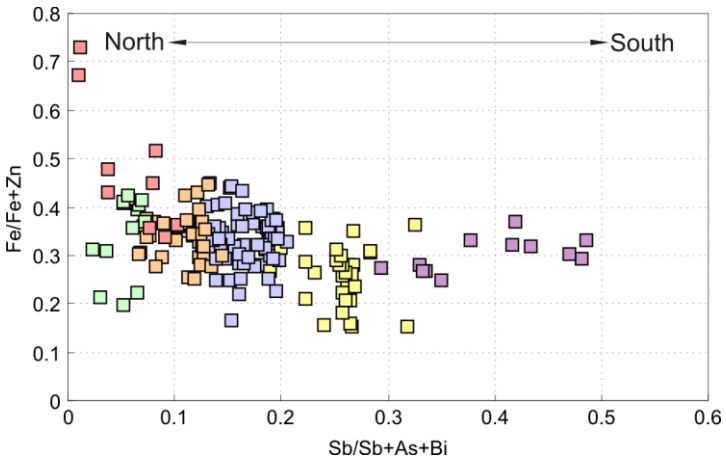

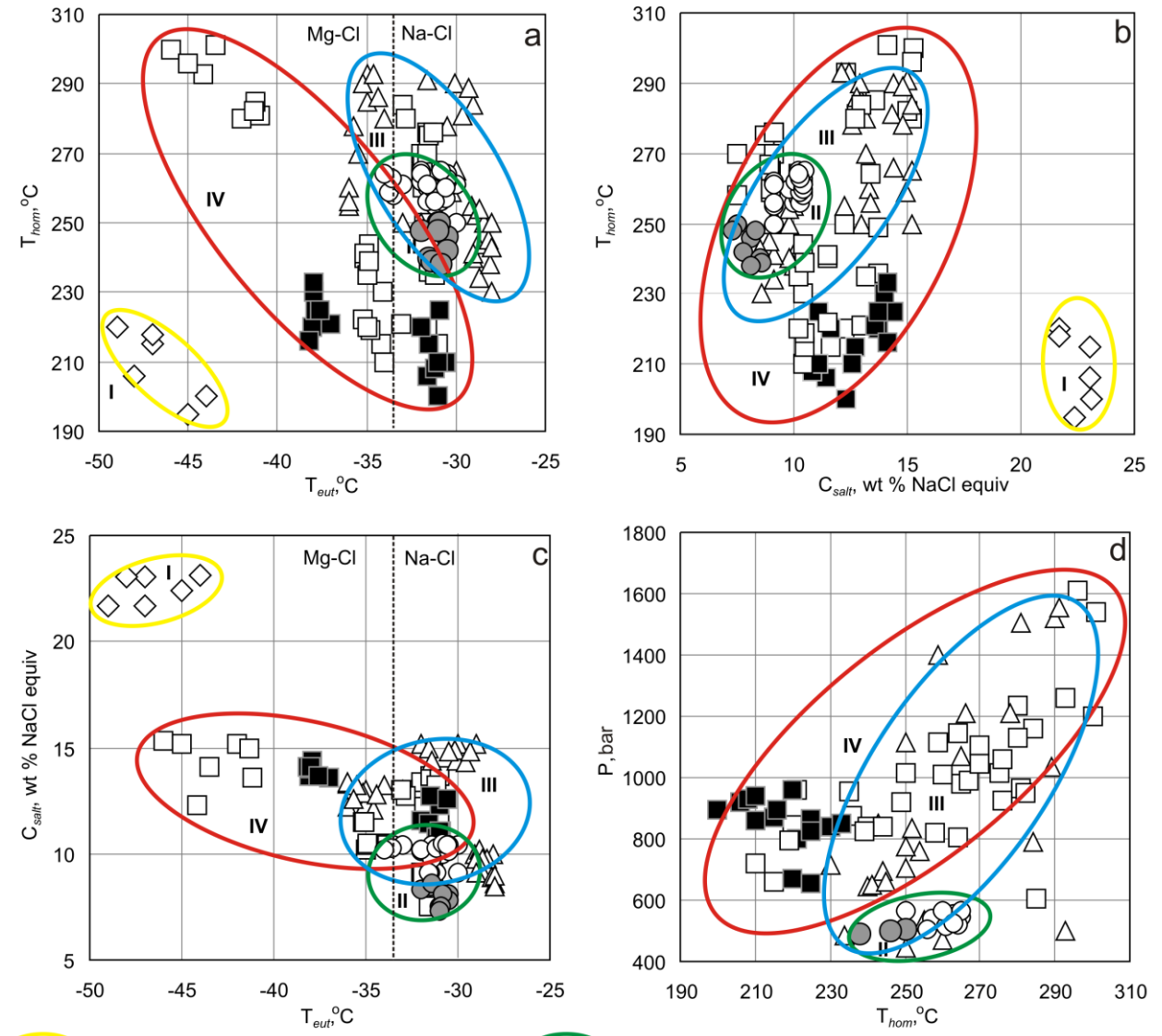

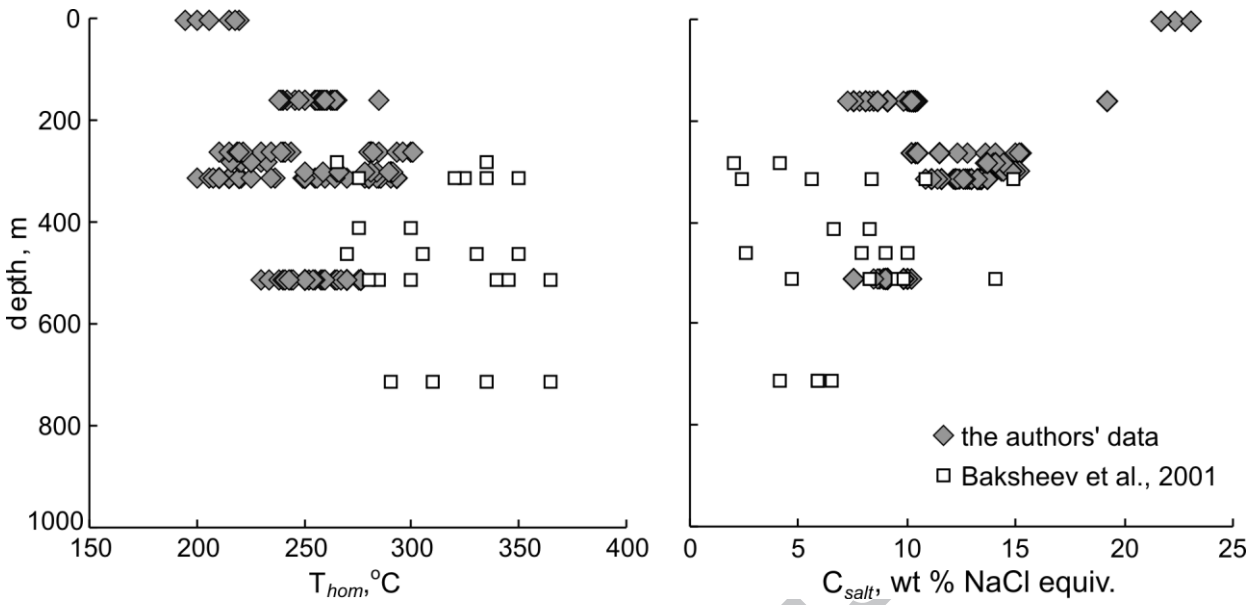

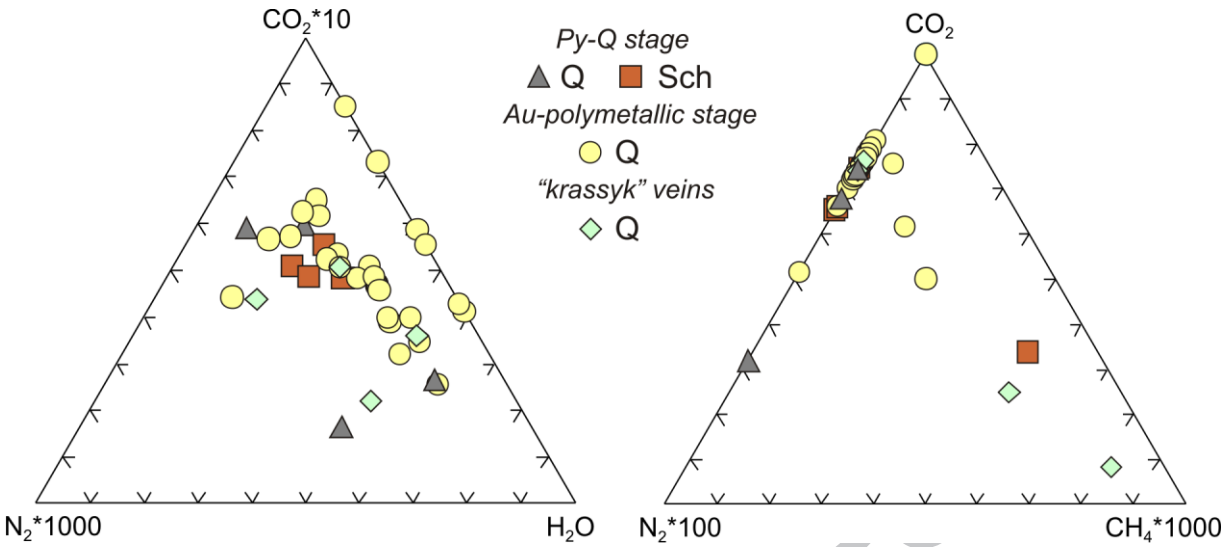

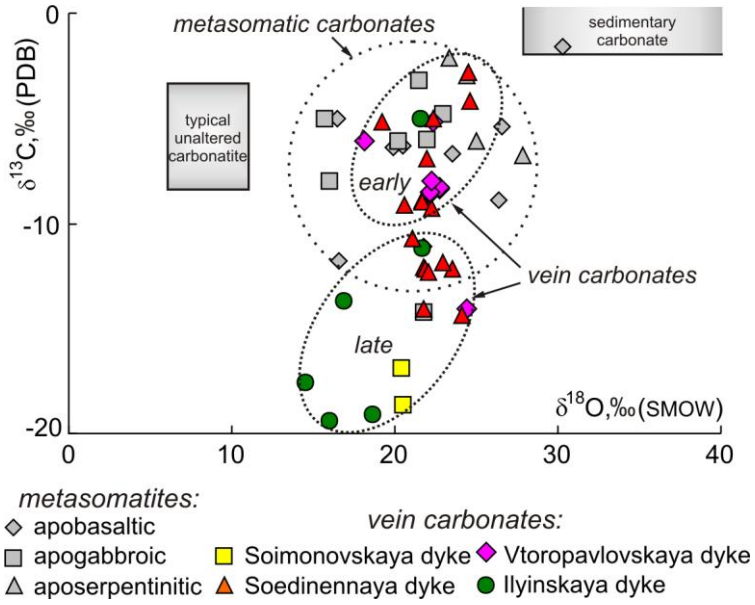

metasomatites:
◇ apobasaltic
□ apogabbroic
△ aposerpentinitic

vein carbonates:
□ Soimonovskaya dyke
◇ Vtoropavlovskaya dyke
△ Soedinennaya dyke
● Ilyinskaya dyke

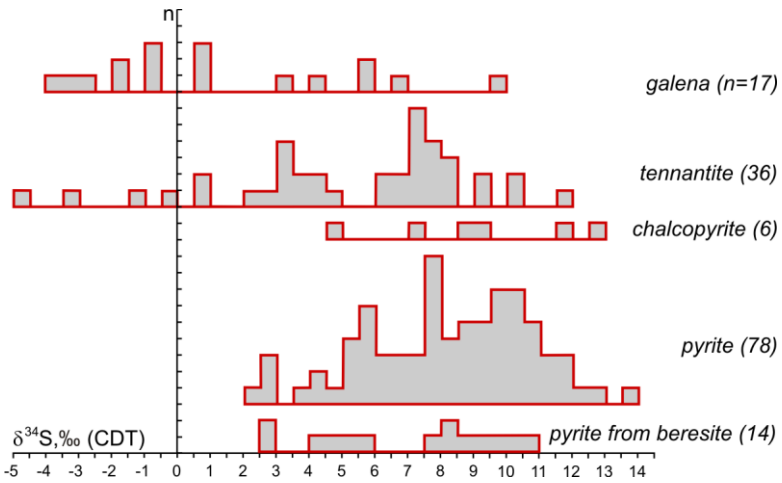

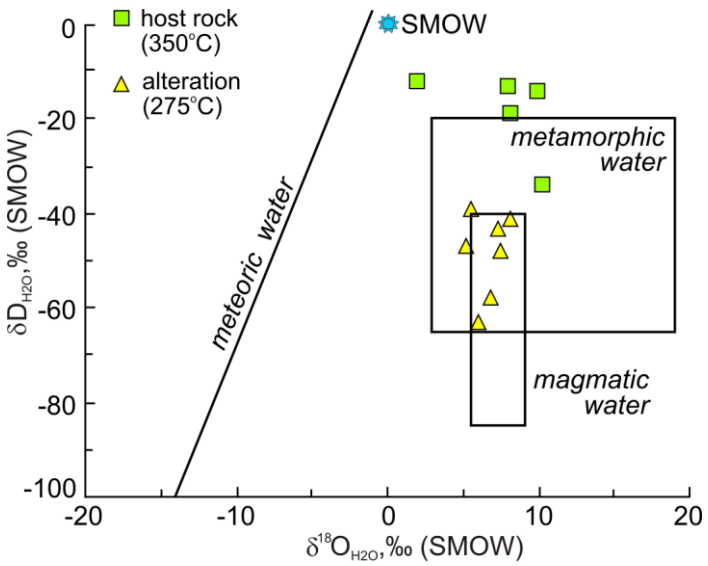

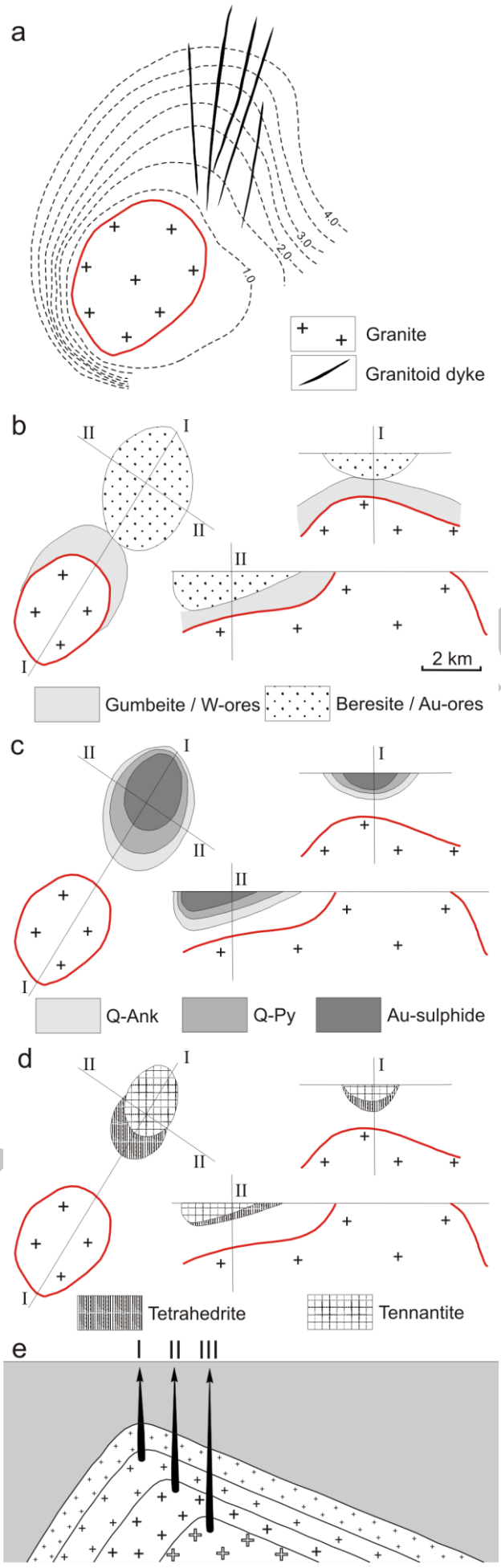

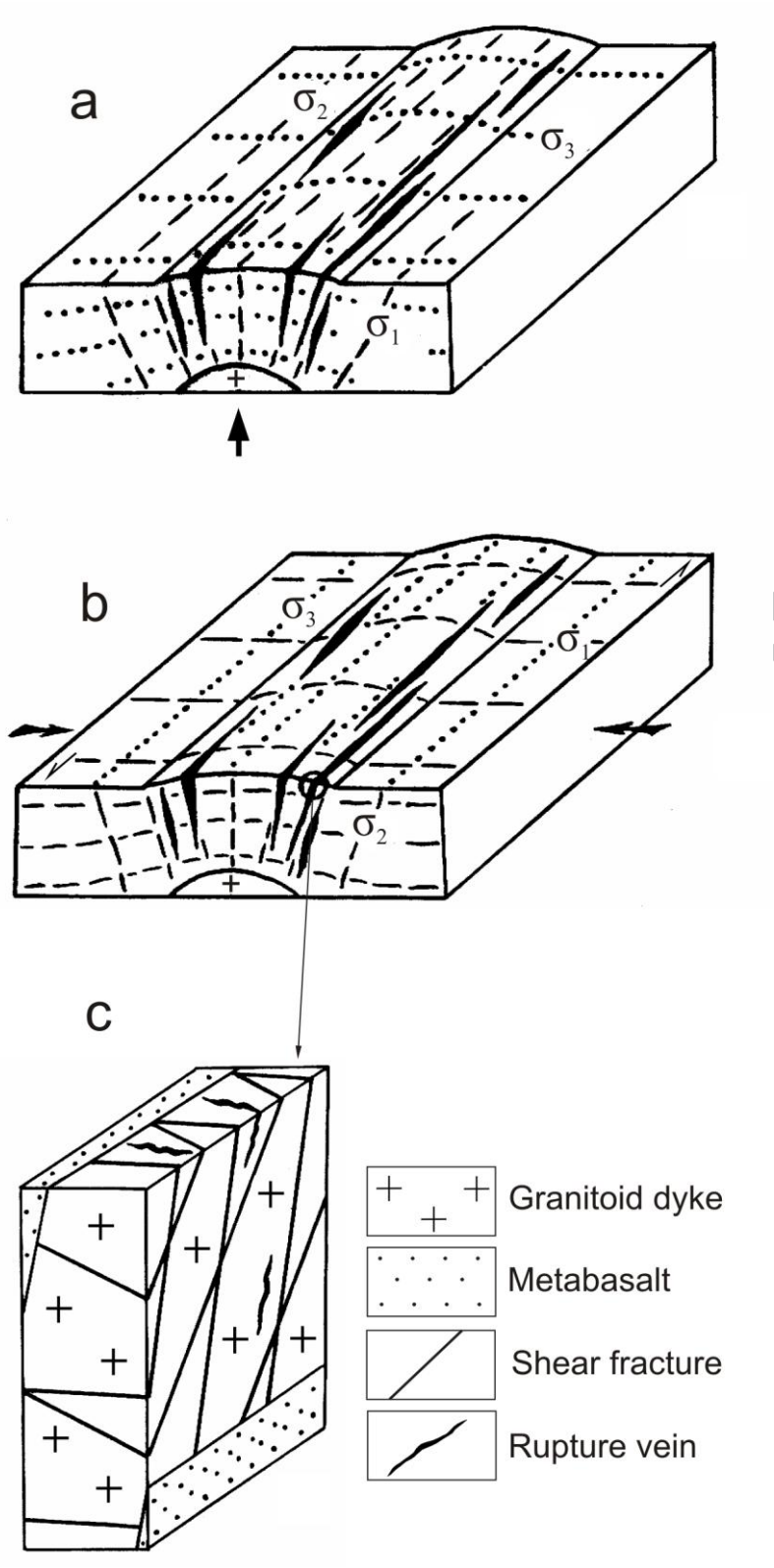

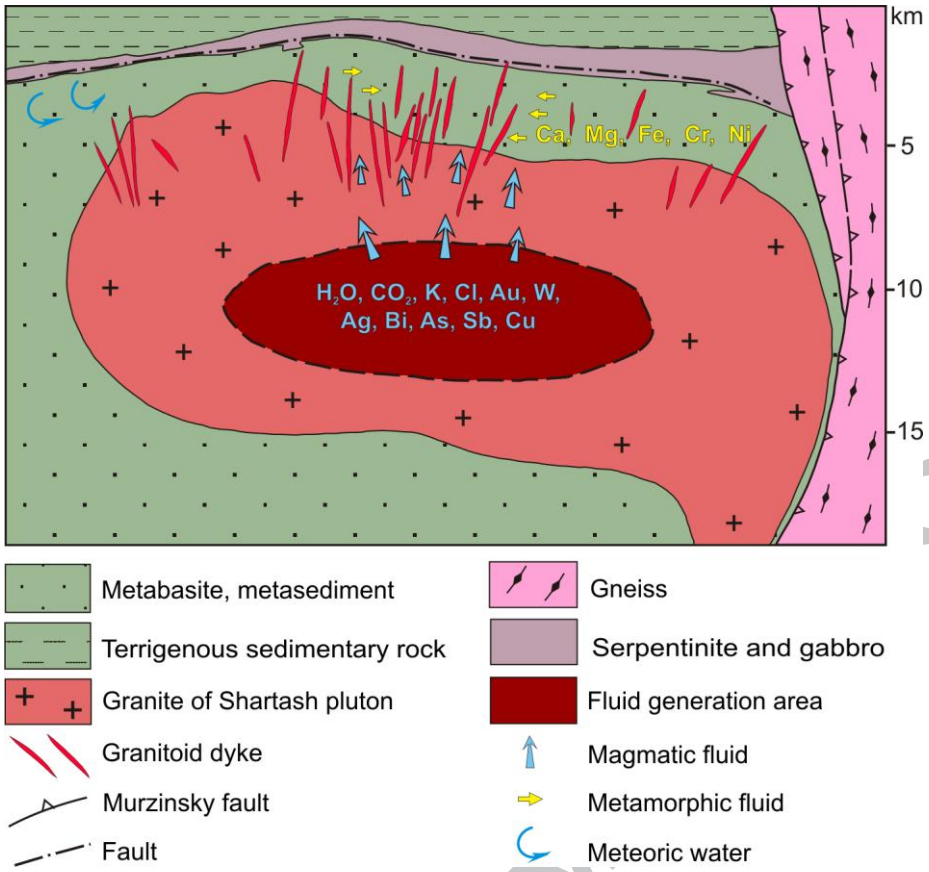

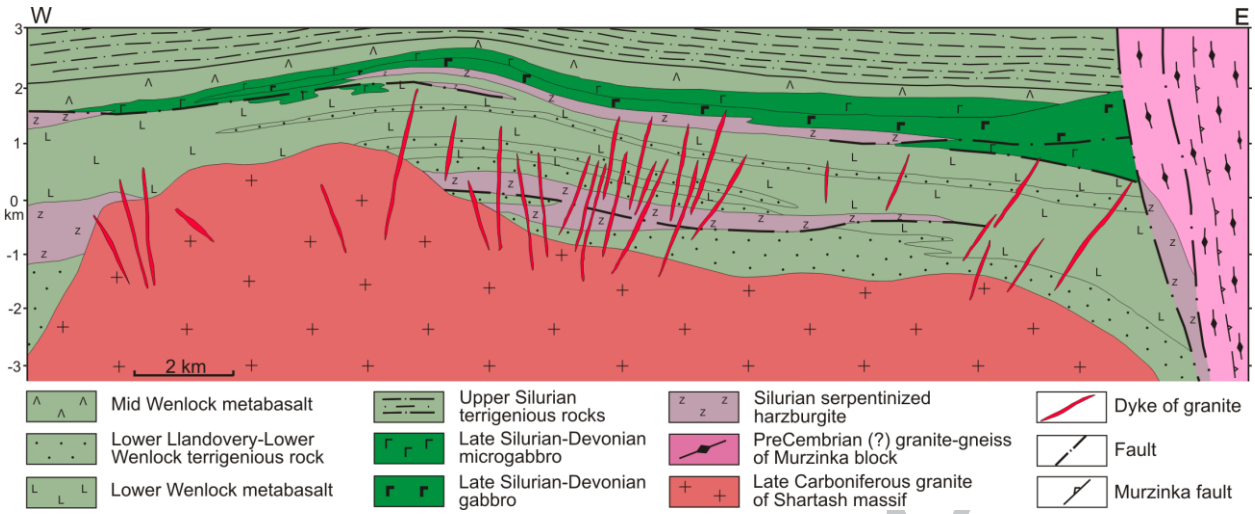

Table 1

The mineral composition of ores from the Berezovsk deposit.

Primary minerals								
Ore minerals					*Gangue minerals*			
1	**pyrite**	FeS_2	28	native bismuth	Bi	1 **quartz**	SiO_2	26	andesine	$(Na,Ca)[Al(Si,Al)Si_2O_8]$
2	**galena**	PbS	29	bornite	Cu_5FeS_4	2 **calcite**	$Ca[CO_3]$	27	microcline	$K[AlSi_3O_8]$
3	**tetrahedrite**	$Cu_{12}Sb_4S_{13}$	30	acanthite	Ag_2S	3 **ankerite**	$Ca(Mg,Fe,Mn)[CO_3]_2$	28	titanite	$CaTiSiO_5$
4	**tennantite**	$Cu_{12}As_4S_{13}$	31	pentlandite	$(Fe,Ni)_9S_8$	4 **tourmaline**	$Na(Fe,Mg)_3Al_6[Si_6O_{18}][BO_3]_3(OH,F)_4$	29	sillimanite	Al_2SiO_5
5	**chalcopyrite**	$CuFeS_2$	32	wittichenite	Cu_3BiS_3	5 **pyrophyllite**	$Al_2[Si_4O_{10}](OH)_2$	30	kyanite	$Al_2(SiO_4)O$
6	**aikinite**	$PbCuBiS_3$	33	bournonite	$PbCuSbS_3$	6 **sericite**	$KAl_2[AlSi_3O_{10}](OH,F)_2$	31	andalusite	$Al_2(SiO_4)O$
7	**scheelite**	$Ca[WO_4]$	34	wolframite	$(Fe,Mn)[WO_4]$	7 dolomite	$CaMg[CO_3]_2$	32	zircon	$ZrSiO_4$
8	**native gold**	Au	35	matildite	$AgBiS_2$	8 magnesite	$Mg[CO_3]$	33	vesuvianite	$Ca_{10}Mg_2Al_4(SiO_4)_5(Si_2O_7)_2(OH)_4$
9	**sphalerite**	ZnS	36	native copper	Cu	9 siderite	$Fe[CO_3]$	34	zoisite	$Ca_2Al_3(SiO_4)(Si_2O_7)(OH)O$
10	pyrrhotite	$Fe_{1-x}S$	37	native lead	Pb	10 paragonite	$NaAl_2[AlSi_3O_{10}](OH,F)_2$	35	clinozoisite	$Ca_2Al_3(SiO_4)(Si_2O_7)(OH)O$
11	molybdenite	MoS_2	38	native platinum	Pt	11 biotite	$K(MgFe)_3[(AlFe)Si_3O_{10}](OH,F)_2$	36	cordierite	$Mg_2Al_2[Si_5O_{18}]$
12	native silver	Ag	39	native iron	Te-Fe	12 talc	$Mg_3[Si_4O_{10}](OH)_2$	37	diopside	$CaMg[Si_2O_6]$
13	hematite	Fe_2O_3	40	emplectite	$CuBiS_2$	13 fuchsite	$K(Al,Cr)_2[AlSi_3O_{10}](OH,F)_2$	38	augite	$(CaNa)(MgFeAlTi)[(SiAl)_2O_6]$
14	magnetite	$FeFe_2O_4$	41	cinnabar	HgS	14 chlorite	$(Fe,Mg,Al)_6[(Al,Si)_4O_{10}](OH)_8$	39	actinolite	$Ca_2(MgFe)_5[Si_8O_{22}](OH)_2$
15	arsenopyrite	Fe[AsS]	42	löllingite	$FeAs_2$	15 epidote	$Ca_2(Fe,Al)Al_2[SiO_4][Si_2O_7]O(OH)$	40	riebeckite	$Na_2(FeMg)_3Fe_2[Si_8O_{22}](OH)_2$
16	cosalite	$Pb_2[Bi_2S_5]$	43	livingstonite	$HgSb_4S_8$	16 fluorite	CaF_2	41	hastingsite	$NaCa_2(FeMg)_4Fe[Si_6Al_2O_{22}](OH)_2$
17	tetradymite	Bi_2Te_2S	44	guanajuatite	Bi_2Se_3	17 anhydrite	$Ca[SO_4]$	42	tremolite	$Ca_2(MgFe)_5[Si_8O_{22}](OH)_2$
18	bismuthinite	Bi_2S_3	45	chromite	$FeCr_2O_4$	18 breunerite	$(Fe,Mg)[CO_3]$	43	antigorite	$(MgFe)_3[Si_2O_5](OH)_4$
19	gersdorffite	Ni[AsS]	46	clinosafflorite	$(Co,Fe,Ni)As_2$	19 adularia	$K[AlSi_3O_8]$	44	sudoite	$Mg_2(AlFe)_3[Si_3AlO_{10}](OH)_8$
20	millerite	NiS	47	galenobismutite	$PbBi_2S_4$	20 albite	$Na[AlSi_3O_8]$	45	natrolite	$Na_2Al_2[Si_3O_{10}]x2H_2O$
21	nickeline	NiAs	48	hessite	Ag_2Te	21 orthoclase	$K[AlSi_3O_8]$	46	phlogopite	$KMg_3(AlSi_3O_{10})(F,OH)_2$
22	polydymite	Ni_3S_4	49	koesterite	$Cu_2(Zn,Fe)SnS_4$	22 rutile	TiO_2	47	geikielite	$MgTiO_3$
23	violarite	Ni_2FeS_4	50	native arsenic	As	23 ilmenite	$FeTiO_3$	48	magnetoplumbite	$(Pb,Mn)(Fe,Mn)_{12}O_{19}$
24	argentite	Ag_2S	51	vaesite	NiS_2	24 apatite	$Ca_5(F,OH)_2[PO_4]_3$	49	chrysotile	$Mg_3(Si_2O_5)(OH)_4$
25	cassiterite	SnO_2	52	freibergite	$Ag_6Cu_4Fe_2Sb_4S_{13}$	25 oligoclase	$(Na,Ca)[Al(Si,Al)Si_2O_8]$	50	grossular	$Ca_3Al_2(SiO_4)_3$
26	teallite	$PbSnS_2$	53	ferberite	$FeWO_4$					
27	electrum	AuAg	54	wulfenite	$Pb(MoO_4)$					
Secondary minerals										
1	malachite	$Cu_2[CO_3](OH)_2$	21	chrysocolla	$Cu_4[Si_4O_{10}](OH)_4x4H_2O$	41	nontronite	$NaFe_2[(SiAl)_4O_{10}](OH)_2xnH_2O$	61	djurleite	$Cu_{31}S_{16}$
2	azurite	$Cu_3[CO_3]_2(OH)_2$	22	scorodite	$Fe[AsO_4]x2H_2O$	42	wulfenite	$Pb[MoO_4]$	62	goethite	α-FeOOH
3	crocoite	$Pb[CrO_4]$	23	caledonite	$Pb_5Cu_2[(CO_3)(SO_4)_3(OH)_6]$	43	ferrimolybdite	$Fe_2[MoO_4]_3x8H_2O$	63	minium	Pb_3O_4
4	pyromorphite	$Pb_5[PO_4]_3Cl$	24	torbernite	$Cu(UO_2)[PO_4]_2x10H_2O$	44	tungstite	WO_3xH_2O	64	brucite	$Mg(OH)_2$
5	cerussite	$Pb[CO_3]$	25	bindheimite	$Pb_2Sb(O,OH,F,H_2O)_7$	45	cuprite	Cu_2O	65	tyrolite	$Ca_2Cu_9(AsO_4)_4(CO_3)(OH)_8x11H_2O$
6	covellite	CuS	26	beudantite	$PbFe_3[(AsO_4)(SO_4)(OH)_6]$	46	phosgenite	$Pb_2[(Cl_2)(CO_3)]$	66	cassedanneite	$Pb_5(CrO_4)_2(VO_4)_2xH_2O$
7	bornite	Cu_5FeS_4	27	phoenicochroite	$Pb_2(CrO_4)O$	47	mimetite	$Pb_5[AsO_4]_3Cl$	67	plumbojarosite	$PbFe_6(SO_4)_4(OH)_{12}$
8	marcasite	FeS_2	28	vauquelinite	$Pb_2Cu(CrO_4)(AsO_4)(OH)$	48	annabergite	$Ni_3[AsO_4]_2x8H_2O$	68	mottramite	$PbCu(VO_4)(OH)$
9	chalcedo	SiO_2	29	embreyite	$Pb_2Cu(CrO_4)(PO_4$	49	morenosite	$Ni[SO_4]x7H_2O$	69	cryptomelane	KMn_8O_{16}

ny		9	)(OH)	9		9	
10 lepidocrocite	γ-FeOOH	30 leadhillite	$Pb_5(CrO_4)_2(PO_4)_2H_2Î$	50 pharmacosiderite	$KFe_4[(AsO_4)_3(OH)_4]x7H_2O$	70 allophane	$Al_2(SiO)_5xnH_2O$
11 chalcocite	Cu_2S	31 linarite	$Pb_4[(SO_4)(CO_3)_2(OH)_2]$	51 massicot	PbO	71 todorokite	$(Mn,Ca,Mg)Mn_2O_7xH_2O$
12 anglesite	$Pb[SO_4]$	32 gypsum	$PbCu[(SO_4)(OH)_2]$	52 plattnerite	PbO_2	72 arsenbrackebuschite	$Pb_2Fe^{3+}(AsO_4)_2(OH)$
13 vanadinite	$Pb_5[VO_4]_3Cl$	33 jarosite	$Ca[SO_4]x2H_2O$	53 cervantite	Sb_2O_4	73 carminite	$PbFe_2(AsO_4)_2(OH)_2$
14 bismutite	$Bi_2[(CO_3)O_2]$	34 bayldonite	$KFe_3[SO_4]_2(OH)_6$	54 senarmontite	Sb_2O_3	74 clinotyrolite	$Ca_2Cu_9(AsO_4,SO_4)_4(OH,O)_{10}x10H_2O$
15 aragonite	$Ca[CO_3]$	35 duftite	$PbCu_3[(AsO_4)(OH)]_2$	55 native sulphur	S_8	75 gaspéite	$NiCO_3$
16 opal	SiO_2xnH_2O	36 cornubite	$PbCu[(AsO_4)(OH)]$	56 smithsonite	$ZnCO_3$	76 <u>bushmakinite</u>	$Pb_2Al(PO_4)(VO_4)(OH)$
17 kaolinite	$Al_2[Si_2O_5](OH)_4$	37 pecoraite	$Cu_5[(AsO_4)_2(OH)_4]$	57 brochantite	$Cu_4[(OH)_6(SO_4)]$	77 xenotime	YPO_4
18 pyrolusite	MnO_2	38 fornacite	$Ni_3[Si_2O_5](OH)_4$	58 langite	$Cu_4(SO_4)(OH)_6x2H_2O$	78 monazite	$(Ce,Nd,Y,Dy,Sm,Nd,Th)(PO_4)$
19 molybdite	MoO_3	39 antlerite	$Cu_3(SO_4)(OH)_4$	59 asentsumebite	$Pb_2Cu[(OH)(SO_4)(AsO_4)]$	79 gartrellite	$Pb(Cu,Fe,Zn)_2(AsO_4,SO_4)_2x2(H_2O,OH)$
20 bismite	Bi_2O_3	40 natrojarosite	$NaFe_3(SO_4)_2(OH)_6$	60 olivenite	$Cu_2[(AsO_4)(OH)]$		

Bold - the main minerals, underline - minerals first found at the Berezovsk deposit. Compiled using Kutyukhin et al. 1947; Kutyukhin 1948; Kleymenov et al. 2005 and authors' data.

Table 2

Chemical composition of native gold from ladder veins at the Berezovsk deposit according to microprobe analysis.

Zoning direction		west → east dykes			north south		depth, m		
		Elizavetin	Vtoropavlov	Soimonov,Ilyin			169-212	262-284	512
Fineness	AuI	941 (1)	863-936 (12) 922	936-984 (7) 954	863-941 (13) 924	936-984 (7) 954	936-984 (8) 952		863-936 (12) 922
	AuII	729-848[a] (14)[c] 797[b]	775-880 (13) 842	757-905 (13) 859	729-861 (20) 805	757-905 (20) 858	729-880 (27) 819	757-905 (13) 859	
Ag, wt%	AuI	5.75	6.28-13.97 7.80	1.39-5.99 4.44	5.75-13.97 7.64	1.39-5.99 4.44	1.39-6.30 4.60		6.28-13.97 7.8
	AuII	14.8-26.71 20.43	11.97-21.63 15.38	9.28-22.91 13.87	13.7-26.71 19.28	9.28-22.91 14.03	11.97-26.71 18.0	9.28-22.91 13.87	
Cu, wt%	AuI	0.26	0.04-0.1 0.06	<0.02-0.13 0.03	0.04-0.26 0.08	<0.02-0.13 0.03	<0.02-0.26 0.06		0.04-0.1 0.06
	AuII	<0.02-0.39 0.07	0.03-0.24 0.14	0.05-1.83 0.37	<0.02-0.39 0.1	0.03-1.83 0.28	<0.02-0.39 0.1	0.05-1.83 0.37	

Note: [a] the range of values, [b] the average value, [c] number of analyses. The separate line for the northern and southern part of the deposit was taken as the middle distance between the Northern and Southern shafts of the Berezovsk mine.

Table 3.
Selected chemical compositions of coexisting tennantite and sphalerite from the Berezovsk deposit (wt %), and their formation temperatures according to geothermometer of Sack and Loucks, 1985.

Sample	Mineral	Ag	Cu	Zn	Fe	Pb	Cd	Sb	As	Bi	S	Se	Mn	Total	T, °C	Formula calculated on the basis 29 apfu (Tnt) and 2 apfu (Sp)
B-23-1	Tnt	0.30	42.83	5.51	2.74	0.10	0.23	3.42	16.98	0.09	28.10	0.10		100.39	166	$(Cu_{10.05}Ag_{0.04})_{10.09}(Zn_{1.26}Fe_{0.73})_{1.99}(As_{3.38}Sb_{0.42})_{3.80}S_{13.06}$
	Sp	0.01	0.60	65.56	0.40		0.74				33.08		-	100.38		$(Zn_{0.98}Fe_{0.01})_{0.99}S_{1.00}$
B-23-2	Tnt	0.36	41.98	6.13	2.18	0.08	0.30	7.65	13.45	0.24	27.49	0.05		99.91	180	$(Cu_{10.08}Ag_{0.05})_{10.13}(Zn_{1.43}Fe_{0.59})_{2.02}(As_{2.74}Sb_{0.96})_{3.70}S_{13.08}$
	Sp	-	0.32	65.55	0.39		0.64				33.10		0.01	100.01		$(Zn_{0.98}Fe_{0.01})_{0.99}S_{1.01}$
B-23-3	Tnt	0.29	41.13	6.47	2.44	-	0.24	6.24	15.52	0.23	28.18	0.08		100.82	180	$(Cu_{9.70}Ag_{0.04})_{9.74}(Zn_{1.48}Fe_{0.65})_{2.13}(As_{3.11}Sb_{0.77})_{3.88}S_{13.18}$
	Sp	0.01	0.38	65.64	0.38		0.71				32.84		-	99.97		$(Zn_{0.98}Fe_{0.01})_{0.99}S_{1.00}$
B-23-4	Tnt	0.36	41.74	5.13	2.99	0.14	0.11	5.57	16.25	0.19	28.16	0.07		100.70	196	$(Cu_{9.84}Ag_{0.05})_{9.89}(Zn_{1.17}Fe_{0.80})_{1.97}(As_{3.25}Sb_{0.68})_{3.93}S_{13.15}$
	Sp	0.01	0.08	65.25	0.65		0.65				33.13		0.02	99.78		$(Zn_{0.97}Fe_{0.01})_{0.98}S_{1.01}$
B-23-5	Tnt	0.34	40.94	5.54	2.71	0.11	0.15	6.30	15.81	0.15	27.80	0.09		99.93	219	$(Cu_{9.76}Ag_{0.05})_{9.81}(Zn_{1.28}Fe_{0.74})_{2.02}(As_{3.20}Sb_{0.78})_{3.98}S_{13.14}$
	Sp	-	0.27	64.76	0.65		0.68				32.90		-	99.25		$(Zn_{0.97}Fe_{0.01})_{0.98}S_{1.01}$
B-25-1	Tnt	0.19	42.46	5.81	2.48	0.07	0.16	3.85	16.53	0.16	27.72	0.07		99.49	197	$(Cu_{10.07}Ag_{0.03})_{10.10}(Zn_{1.34}Fe_{0.67})_{2.01}(As_{3.33}Sb_{0.48})_{3.81}S_{13.04}$
	Sp	-	1.32	64.88	0.44		0.65				32.65		-	99.94		$(Zn_{0.97}Fe_{0.01})_{0.98}S_{1.00}$
B-25-2	Tnt	0.23	41.43	6.15	2.21	0.09	0.08	5.05	16.19	0.23	28.22	0.07		99.94	213	$(Cu_{9.80}Ag_{0.03})_{9.83}(Zn_{1.41}Fe_{0.60})_{2.01}(As_{3.25}Sb_{0.62})_{3.87}S_{13.24}$
	Sp	0.01	0.57	65.14	0.44		0.69				33.07		0.01	99.94		$(Zn_{0.97}Fe_{0.01})_{0.98}S_{1.01}$
B-25-3	Tnt	0.16	42.69	5.82	2.52	0.19	0.14	4.01	16.36	0.27	27.83	0.04		100.00	220	$(Cu_{10.09}Ag_{0.02})_{10.11}(Zn_{1.34}Fe_{0.68})_{2.02}(As_{3.28}Sb_{0.49})_{3.77}S_{13.04}$
	Sp	-	0.51	65.74	0.54		0.80				33.01		-	100.61		$(Zn_{0.98}Fe_{0.01})_{0.99}S_{1.00}$
B-25-4	Tnt	0.24	42.54	5.19	3.12	0.12	0.18	3.84	16.73	0.22	27.76	0.12		100.04	246	$(Cu_{10.05}Ag_{0.03})_{10.08}(Zn_{1.19}Fe_{0.84})_{2.03}(As_{3.35}Sb_{0.47})_{3.82}S_{12.99}$
	Sp	0.01	1.06	65.42	0.88		0.81				32.02		0.02	100.22		$(Zn_{0.98}Fe_{0.02})_{1.00}S_{0.98}$
B-25-5	Tnt	0.21	42.67	5.48	2.89	0.11	0.06	3.42	16.74	0.20	27.83	0.15		99.76	298	$(Cu_{10.08}Ag_{0.03})_{10.11}(Zn_{1.26}Fe_{0.78})_{2.04}(As_{3.35}Sb_{0.42})_{3.77}S_{13.03}$
	Sp	0.02	1.11	65.12	1.01		0.65				32.42		0.01	100.34		$(Zn_{0.97}Fe_{0.02})_{0.99}S_{0.99}$
B-44-1	Tnt	0.33	42.54	5.69	2.57	0.11	0.20	4.13	16.04	0.05	27.97	0.08		99.70	123	$(Cu_{10.06}Ag_{0.05})_{10.11}(Zn_{1.31}Fe_{0.69})_{2.00}(As_{3.22}Sb_{0.51})_{3.73}S_{13.11}$
	Sp	-	0.36	66.01	0.25		0.74				32.94		-	100.30		$(Zn_{0.98}Fe_{\cdot})_{0.99}S_{1.00}$
B-44-2	Tnt	0.21	42.69	6.27	2.21	0.08	0.19	4.09	16.24	0.04	28.08	-		100.10	143	$(Cu_{10.05}Ag_{0.03})_{10.08}(Zn_{1.44}Fe_{0.59})_{2.03}(As_{3.24}Sb_{0.50})_{3.74}S_{13.11}$
	Sp	0.01	0.40	65.73	0.24		0.71				32.85		-	99.94		$(Zn_{0.98}Fe_{\cdot})_{0.99}S_{1.00}$
B-44-3	Tnt	0.29	42.52	6.28	2.45	0.09	0.08	4.36	15.84	0.05	28.06	0.04		100.06	182	$(Cu_{10.02}Ag_{0.04})_{10.06}(Zn_{1.44}Fe_{0.66})_{2.10}(As_{3.17}Sb_{0.54})_{3.71}S_{13.11}$
	Sp	-	0.80	65.62	0.37		0.70				32.89		-	100.39		$(Zn_{0.98}Fe_{0.01})_{0.99}S_{1.00}$
B-44-4	Tnt	0.25	42.44	5.80	2.39	0.11	0.17	4.36	15.89	0.01	28.09	0.09		99.59	204	$(Cu_{10.04}Ag_{0.03})_{10.07}(Zn_{1.33}Fe_{0.64})_{1.97}(As_{3.19}Sb_{0.54})_{3.73}S_{13.17}$
	Sp	0.01	0.87	65.44	0.47		0.63				32.78		-	100.20		$(Zn_{0.98}Fe_{0.01})_{0.99}S_{1.00}$
B-44-5	Tnt	0.34	40.97	7.42	1.98	0.10	0.05	5.95	15.04	0.08	27.61	0.08		99.61	253	$(Cu_{9.79}Ag_{0.05})_{9.84}(Zn_{1.72}Fe_{0.54})_{2.26}(As_{3.05}Sb_{0.74})_{3.79}S_{13.08}$
	Sp	-	0.30	65.94	0.44		0.68				33.29		0.01	100.66		$(Zn_{0.98}Fe_{0.01})_{0.99}S_{1.01}$
B-26-1	Tnt	0.13	42.94	5.35	2.89	0.10	0.13	2.56	17.68	0.20	27.97	0.08		100.04	149	$(Cu_{10.08}Ag_{0.02})_{10.10}(Zn_{1.22}Fe_{0.77})_{1.99}(As_{3.52}Sb_{0.31})_{3.83}S_{13.02}$

	Sp	-	1.20	65.08	0.35		0.50				32.19		-	99.32		$(Zn_{0.98}Fe_{0.01})_{0.99}S_{0.99}$
B-26-2	Tnt	0.21	42.31	5.59	2.88	0.06	0.13	3.34	17.49	0.24	27.53	0.15		99.92	172	$(Cu_{10.01}Ag_{0.03})_{10.04}(Zn_{1.29}Fe_{0.77})_{2.06}(As_{3.51}Sb_{0.41})_{3.92}S_{12.91}$
	Sp	-	1.47	64.63	0.42		0.53				32.48		-	99.52		$(Zn_{0.97}Fe_{0.01})_{0.98}S_{1.00}$
B-26-3	Tnt	0.13	42.73	5.63	2.66	0.05	0.11	2.43	17.77	0.24	28.04	0.13		99.90	192	$(Cu_{10.04}Ag_{0.02})_{10.06}(Zn_{1.28}Fe_{0.71})_{1.99}(As_{3.540}Sb_{0.30})_{3.848}S_{13.06}$
	Sp	0.02	1.84	63.88	0.46		0.47				32.56		0.01	99.23	7	$(Zn_{0.96}Fe_{0.01})_{0.97}S_{1.00}$
B-26-4	Tnt	0.16	42.79	5.68	2.65	0.12	0.07	2.31	17.95	0.25	28.02	0.20		100.20	209	$(Cu_{10.03}Ag_{0.02})_{10.05}(Zn_{1.29}Fe_{0.71})_{2.00}(As_{3.57}Sb_{0.28})_{3.85}S_{13.02}$
	Sp	-	0.88	65.66	0.50		0.47				33.38		0.03	100.91		$(Zn_{0.97}Fe_{0.01})_{0.98}S_{1.00}$
B-26-5	Tnt	0.13	42.72	6.26	2.19	0.10	0.06	2.59	17.79	0.25	27.85	0.18		100.11	210	$(Cu_{10.05}Ag_{0.02})_{10.07}(Zn_{1.43}Fe_{0.59})_{2.02}(As_{3.55}Sb_{0.32})_{3.87}S_{12.98}$
	Sp	-	1.42	65.00	0.37		0.55				32.70		-	100.04		$(Zn_{0.97}Fe_{0.01})_{0.89}S_{1.01}$

-: Concentration below detection limit (analysis wt.%); blank: not analysed. Tnt – tennantite, Sp – sphalerite.

Table 4
Chemical composition (wt%) of selected Bi minerals and sulphides from the Berezovsk deposit.

Mineral	Ag	Cu	Pb	Fe	Zn	Cd	Sb	Te	Bi	S	Au	Total	*n*	Formula calculated on the basis *n* apfu
Matildite	23.21	4.68							56.06	16.53		100.48	4	$Ag_{0.80}Cu_{0.27}Bi_{1.00}S_{1.92}$
	23.50	3.37							56.41	17.36		100.64	4	$Ag_{0.81}Cu_{0.20}Bi_{1.00}S_{2.00}$
	24.81	2.33							54.61	17.24		98.99	4	$Ag_{0.86}Cu_{0.14}Bi_{0.98}S_{2.02}$
	22.92	4.11							54.96	17.53		99.52	4	$Ag_{0.78}Cu_{0.24}Bi_{0.97}S_{2.01}$
	26.02	1.08							55.42	16.63		99.15	4	$Ag_{0.93}Cu_{0.07}Bi_{1.02}S_{1.99}$
	22.45	7.75							52.33	17.04		99.57	4	$Ag_{0.75}Cu_{0.44}Bi_{0.90}S_{1.91}$
Aikinite	-	10.02	31.40						41.96	16.84		100.22	6	$Pb_{0.88}Cu_{0.91}Bi_{1.16}S_{3.04}$
	-	11.52	35.09						37.56	16.54		100.71	6	$Pb_{0.97}Cu_{1.04}Bi_{1.03}S_{2.96}$
	-	10.94	33.76						39.53	17.02		101.25	6	$Pb_{0.93}Cu_{0.98}Bi_{1.08}S_{3.02}$
	-	11.28	31.23						39.98	16.86		99.35	6	$Pb_{0.87}Cu_{1.02}Bi_{1.10}S_{3.02}$
	0.53	10.60	32.65						40.17	16.65		100.60	6	$Pb_{0.93}Cu_{0.96}Ag_{0.03}Bi_{1.11}S_{2.99}$
Chalcopyrite I	0.17	33.69		31.19						36.33	-	101.38	4	$Cu_{0.97}Fe_{0.95}S_{2.07}$
	0.18	27.01		37.55						35.60	-	100.34	4	$Cu_{0.79}Fe_{1.16}S_{2.05}$
Chalcopyrite II	0.08	34.57		29.65						35.15	0.32	99.77	4	$Cu_{1.02}Fe_{0.93}S_{2.05}$
	-	34.77		29.78						35.09	0.05	99.62	4	$Cu_{1.02}Fe_{0.93}S_{2.05}$
Galena I	0.10	-	85.67	-			0.07	0.01	-	13.34		99.19	2	$Pb_{0.99}Sb_{0.001}Ag_{0.002}S_{1.00}$
	0.16	-	85.26	-			0.06	-	-	13.03		98.51	2	$Pb_{1.00}Sb_{0.001}Ag_{0.004}S_{0.99}$
Galena II	1.24	-	82.91	-			-	0.09	2.83	13.41		100.47	2	$Pb_{0.95}Bi_{0.03}Ag_{0.03}S_{0.99}$
	0.95	-	82.96	-			-	0.07	2.28	13.37		99.62	2	$Pb_{0.96}Bi_{0.03}Ag_{0.02}S_{1.00}$
Sphalerite I		0.17		0.38	67.07	0.78				31.58		99.98	2	$Zn_{1.01}Fe_{0.01}Cd_{0.01}Cu_{0.003}S_{0.97}$
		0.36		0.30	64.99	0.90				32.94		99.49	2	$Zn_{0.97}Fe_{0.01}Cd_{0.01}Cu_{0.01}S_{1.01}$
Sphalerite II		1.70		0.40	67.16	0.53				31.08		100.87	2	$Zn_{1.01}Fe_{0.01}Cd_{0.01}Cu_{0.03}S_{0.95}$
		0.58		0.18	66.50	0.62				32.99		100.87	2	$Zn_{0.97}Fe_{0.003}Cd_{0.01}Cu_{0.01}S_{1.00}$

-: Concentration below detection limit (analysis wt.%); blank: not analysed.

Table 5
Microthermometric study of individual fluid inclusions (FI) in minerals from the ore veins at the Berezovsk deposit

Sample/ mineral	Type of FI	*n*	T_{hom}, °C	T_{eut}, °C	$T_{m(ice)}$, °C	$T_{melt.\ clathrate}$, °C	$T_{meltCO2}$, °C	T_{homCO2}, °C	C_{salt}, wt% NaCl equiv	D, g/cm^3	P, bar
Early quartz-tourmaline vein											
Б-47 Q	III	8	195…220	-49…-44.1	-21…-19				21.7…23.0		
Ankerite-quartz stage											
E-16	I	14	250…264	-32…-30.1		4…5	-56.9…-56.7	28…29.9	9.1…10.4	0.51…0.55	542…566
Q	II	13					-56.9…-56.7	28…30			
E-17	I	18	256…264	-34…-30.2		3.8…4.3	-57.2…-56.8	24…30.1	9.2…10.4	0.5…0.6	515…566
Q	II	10					-57.1…-56.8	24…30			
E-17	I	9	238…250	-32…-30.5		5.3…6.1	-57.2…-56.7	23…24.2	7.3…8.6	0.5…0.6	489…500
Ank	III	8					-57.2…-56.8	18.3…20.1			
	II	9					-57.1…-56.8	20…23.6			
Pyrite-quartz stage											
Б-70	I	13	230…255	-29.1…-28.1		4.2…5.4	-58.2…-57.9	20…26	8.6…10.2	0.61…0.7	484…851
Q	II	18					-58.1…-57.9	22…25.4			
Б-26а	I	12	250…293	-36.0…-33.0		1.8…2.6	-62.8…-63.4	0.8…4.0	12.8…13.4	0.46…0.5	445…530
Q	III	7		-36.0…-33.5		2.0	-62.7…-62.9		13.0		
	II	10					-63.0…-63.5	1.0…3.7			
Gold-polymetallic stage											
Б-44	I	12	250…291	-32.0…-29.6		0.5…1.1	-58.0…-57.3	4.3…22.7	15.2…14.4	0.62…0.85	789…1504
Q	II	5					-57.9…-57.2	10.1…23.0			

Б-54	I	11	258…276	-32…-31	4.2…6	-57.8…-57	19…22	7.5…10.2	0.66…0.78	818…1060
Q	II	11				-57.6…-57	20…21.5			
Б-35	I	12	210…240	-35.2…-34	3.2…4.4	-56.9…-56.7	21…24	10.2…11.5	0.69…0.71	720…841
Q	II	11				-56.9…-56.7	21.5…24			
Б-23б	I	9	280…301	-46.0…-41.0	0.3…1.2	-58.5…-57.9	1.5…20	12.8…15.3	0.53…0.84	607…1609
Q	II	10				-58.0…-57.9	5.0…11.7			
Б-26	I	13	215..284	-32.0…-30.6	1.6…3.0	-57.5…-57.0	17.5…25.0	12.2…11.6	0.63…0.75	658…1162
Q	II	4					18.3…19.3			
Б-26	I	6	200…225	-32.0…-30.6	2.2…3.6	-57.5…-57.0	17.0…19.4	12.3…10.8	0.73…0.78	864…958
Sp	II	5				-57.0	17.3…19			
Б-25а	I	11	220…233	-38.2…-37	1…1.6	-57.2…-57.0	21.9…25.1	14.4…13.6	0.63…0.71	654…893
Sp	II	14				-57.7…-57.1	21.0…25.0			

Type of FI: I – liquid H_2O + liquid CO_2 + vapor CO_2, II – vapor CO_2-rich, III – liquid H_2O + vapor H_2O. Minerals: Q – quartz, Ank – ankerite, Sp – sphalerite.

Table 6
Stable isotope composition of minerals from alteration halos at the Berezovsk ore field.

Zone of alteration halo	Sample	Mineral	$\delta^{18}O$, ‰	$\delta^{13}C$, ‰	δD, ‰
Profile 1: Alteration of basalt					
0 - host basalt	403SHM	epidote	+3.0		-48
		actinolite	+9.1		-58
		chlorite	+7.3		-57
		calcite	+16.5	-5.0	
1 - propilitic basalt	254/107	chlorite	+9.2		-58
		ankerite	+20.5	-6.3	
		calcite	+30.3	-1.6	
2 - quartz-sericite-albite-chloritic metasomatic rock	254/104.6	chlorite	+8.6		-61
		ankerite	+26.4	-8.9	
		calcite	+19.9	-6.4	
3 - quartz-sericite-carbonate-albitic metasomatic rock	254/100	sericite	+11		-48
		muscovite	+8.7		-47
		breunnerite	+23.5	-6.7	
		ankerite	+21.8	-11.1	
4 - listvenite	254/95	sericite	+10.8		-43
		magnesite	+26.6	-5.4	
		ankerite	+22.2	-8.7	
		calcite	+16.6	-11.8	
Profile 2: Alteration of gabbro					
0 - gabbro	58-BR	amphibole	+7.1		-87
	58-BR-II	ankerite	+21.5	-3.2	
1 - quartz-sericite-muscovite-carbonatic metasomatic rock	57-BR	chlorite	+6.4		-59
		ankerite	+15.7	-5.0	
	57-BR-I	ankerite	+22.9	-4.8	
2 - “grey” listvenite (quartz-carbonatic metasomatic rock)	IV56a-BR	ankerite	+22.0	-6.0	
	56a-BR	breunnerite	+16.0	-8.0	
3 - “green”listvenite (fuchsite-quartz-carbonatic metasomatic rock)	54-BR	fuchsite	+9.5		-63
		ankerite	+20.2	-6.1	
Profile 3: Alteration of serpentinite					
0 - host chrysotile serpentinite	IX-KR	serpentine	+9.5		-78
1 - antigorite serpentinite	VIII-KR	serpentine	+7.4		-63
		breunnerite	+21.8	-14.2	
2 - talc-carbonatic metasomatic rock	VII-KR	breunnerite	+23.3	-2.1	
3 - “grey” listvenite (quartz-carbonatic metasomatic rock)	VI-KR	breunnerite	+25.0	-6.1	
4 - “green” listvenite (fuchsite-quartz-carbonatic metasomatic rock)	IVb-KR	breunnerite	+27.8	-6.8	
	IVa-KR	breunnerite	+24.4	-3.0	
		fuchsite	+10.4		-58

Table 7
Comparison of the Berezovsk deposit with orogenic and intrusion-related gold deposits (IRGD).

Specific features	IRGD	Orogenic deposits	Berezovsk deposit
Tectonic setting	Ancient continental margin behind accretionary or collisional orogen and subduction-related magmatic arc	Accretionary and collisional orogens, at or above the brittle-ductile transition, in compressional settings	Active continental margin evolved to collisional regime
Host rock	Igneous rocks (associated with aplite and/or pegmatite)	Metamorphic rocks (greenschist to amfibolite facies)	Granitoids dykes and metavolcano-sedimentary rocks
Relationship with intrusion	Spatial and/or temporal relationship with I-type granitic plutons with evidences of hydrothermal fluid generation (porphyric texture, aplite and/or pegmatite dykes, greisen/skarn alteration)	Sometimes spatial relationship with granitic pluton, but radiometric age determinations suggest time gap between intrusion and veins	Spatial relationship with I-type granitic Shartash massif
Wall-rock alteration	Weak to moderate (potassic, phyllic, greisen, carbonation, sulphidation)	Carbonate-sulphide±sericite±chlorite	Beresitisation (quartz+ankerite+sericite+pyrite±fuchsite)
Mineralisation styles	Sheeted veins and stockworks, skarns, replacements, breccias, disseminations	Linear tensional vein systems	Vein system and disseminated mineralization in altered wall rock
Metal assemblage	Au, Bi, Te, W, Mo, B, Ag, As, Sb, Sn with low base metals	Au, Ag, As, Sb, S	Au, Ag, Bi, As, Sb, W
Mineral assemblage	Reduced (arsenopyrite, pyrrhotite, pyrite, but no magnetite or hematite)	Pyrrhotite, pyrite, arsenopyrite, chalcopyrite, galena	Pyrite, galena, tennantite, aikinite, chalcopyrite, native gold, sphalerite
Sulphide content	<5 vol.%	≤3-5 vol.% (mainly Fe-sulphide)	≤10 vol.% (commonly 3-5 vol.%)
Metal zoning: lateral	Temperature-dependent concentric metal zones surrounding cooling plutons (Au-Bi-Te±W → As-Sb-Au → Ag-Pb-Zn)	Mineral and metal zoning is poorly developed or absent	Mineral and metal zoning relative to roof of the Shartash massif
vertical	W±Mo at depth and Au-Bi at shallower levels	Lack of zoning	W-ore at depth and Au-ore at shallower levels
Ore fluid	H_2O-CO_2±CH_4	H_2O-CO_2±CH_4	H_2O-CO_2±CH_4-NaCl
salinity	From high to low salinity: 5-40 wt% NaCl equiv.	Low salinity: 3-7 wt% NaCl equiv. with Na>K≥Ca,Mg	7.3-18.2 wt% NaCl equiv.
T,°C	400-200	650-200	300-230
P, kbar	0.5-1.5	1-5	0.3-2.3 (mostly 0.5-1.2)
CH_4 content	Significant	Significant	Insignificant
CO_2 content	High	High, typically 5-20 mol.% CO_2	High
N_2 content	Insignificant	Significant	Insignificant
pH	Acidic	Near-neutral ~5.5	Acidic
Depth of mineralisation	From deeper to shallow crustal environment	Epizonal (<6 km), mesozonal (6-12 km), hypozonal (>12 km)	3-4.5 km
Sources of fluids	Product of local-scale fluid convection likely derived from and driven by a cooling magmatic body	Result from crustal-scale fluid flow likely derived from metamorphic dehydration	Magmatic fluid evolving in the result of phase separation and mixing with fluid derived from decarbonation and dehydration of host rock and with meteoric water
Timing	Mineralisation and associated causative pluton are coeval (events are within 2 million years)	Predominant synchronous with deformation and metamorphism	Synchronous with magmatic events
Calculated $\delta^{18}O_{H2O}$ (‰)	+5…+10‰	+5…+10‰ (+5…+8 Archaean, +7…+10 Phanerozoic)	+3…+9.6‰

Compiled using Groves et al., 1998; Sillitoe and Thompson, 1998; Thompson et al., 1999; Lang et al., 2000; Ridley and Diamond, 2000; Thompson and Newberry, 2000; Hart and Goldfarb, 2005; Hart, 2005, 2007; Goldfarb et al., 2005; McKay and Wake, 2006; Kontak and Kyser, 2011; Tomkins, 2013; Goldfarb and Groves, 2015 and authors' data.

The Berezovsk deposit is the oldest gold mine in the Urals and in Russia and is still in production.

Mineral and metal zoning occurs in the roof of the Shartash granite massif.

Gold ores were formed at 300-230°C and 0.3-2.3 kbar (mostly 0.5-1.2) from the H_2O-CO_2-CH_4-NaCl fluid with salinity 7.3-18.2 wt % NaCl equiv.

Magmatic fluid evolved as a result of phase separation and mixing with fluid derived from decarbonation and dehydration of host rock and with meteoric water.